Rich band structure and multiple long-lived isomers in the odd-odd ^{118}Cs nucleus

K. K. Zheng,[1,2] C. M. Petrache,[1] Z. H. Zhang,[3] A. Astier,[1] B. F. Lv,[1,*] P. T. Greenlees,[4] T. Grahn,[4] R. Julin,[4] S. Juutinen,[4] M. Luoma,[4] J. Ojala,[4] J. Pakarinen,[4] J. Partanen,[4,†] P. Rahkila,[4] P. Ruotsalainen,[4] M. Sandzelius,[4] J. Sarén,[4] H. Tann,[4,5] J. Uusitalo,[4] G. Zimba,[4] B. Cederwall,[6] Ö. Aktas,[6] A. Ertoprak,[6] W. Zhang,[6] S. Guo,[2,7] M. L. Liu,[2,7] X. H. Zhou,[2,7] I. Kuti,[8] B. M. Nyakó,[8] D. Sohler,[8] J. Timár,[8] C. Andreoiu,[9] M. Doncel,[5] D. T. Joss,[5] and R. D. Page[5]

[1]*Université Paris-Saclay, CNRS/IN2P3, IJCLab, 91405 Orsay, France*

[2]*Key Laboratory of High Precision Nuclear Spectroscopy and Center for Nuclear Matter Science, Institute of Modern Physics, Chinese Academy of Sciences, Lanzhou 730000, People's Republic of China*

[3]*Mathematics and Physics Department, North China Electric Power University, Beijing 102206, China*

[4]*University of Jyväskylä, Department of Physics, P.O. Box 35, FI-40014, University of Jyväskylä, Finland*

[5]*Oliver Lodge Laboratory, Department of Physics, University of Liverpool, Liverpool L69 7ZE, United Kingdom*

[6]*KTH Department of Physics, S-10691 Stockholm, Sweden*

[7]*School of Nuclear Science and Technology, University of Chinese Academy of Science, Beijing 100049, People's Republic of China*

[8]*Institute for Nuclear Research (Atomki), 4001 Debrecen, Hungary*

[9]*Department of Chemistry, Simon Fraser University, Burnaby, BC V5A 1S6, Canada*

(Received 12 May 2021; accepted 8 October 2021; published 21 October 2021)

One of the largest sets of collective excitations built on two-quasiparticle configurations in odd-odd nuclei of the proton-rich $A \approx 120$ mass region is reported in ^{118}Cs. Several new rotational bands and long-lived isomers have been identified. The 8^+ bandhead of the $\pi h_{11/2} \otimes \nu h_{11/2}$ band is a short-lived isomer with a half-life in the nanosecond range, while the 7^+ state below it is a long-lived isomer with a half-life of $T_{1/2} = 0.55(6)$ μs. Two other long-lived isomers have been identified: a 66-keV transition detected at the MARA focal plane depopulates one of them, indicating a half-life in the microsecond range, while no depopulating transitions have been identified for the other, indicating a much longer half-life. Extensive particle number conserving cranked shell model calculations and alignment analysis have been employed to investigate the rich band structure of ^{118}Cs, which exhibits one of the most complete sets of two-quasiparticle configurations in nuclei close to the proton drip line.

DOI: 10.1103/PhysRevC.104.044325

I. INTRODUCTION

The recent spectroscopic studies of cesium nuclei have focused on chirality, which was observed in a long sequence of odd-odd nuclei from ^{122}Cs to ^{132}Cs [1]. The odd-even Cs nuclei have been the object of investigations devoted to the evolution of the collective properties far from stability [2]. However, the study of the band structures of the lightest Cs nuclei is confronted with the increasing difficulty to populate high-spin states using fusion-evaporation reactions, due to the limited choice of projectile-target combinations which lead to small cross sections for the evaporation of neutrons close to the proton drip line. The existing experimental information on high-spin states in very-proton-rich nuclei is therefore increasingly scarce towards the proton-drip line. This prohibits a detailed comparison between the experimental data and theoretical calculations employing different interactions. The lightest odd-odd nucleus in the Cs chain with a known rich band structure is ^{120}Cs, in which five band structures have been observed [3,4]. In the lighter ^{112,114,116,118}Cs nuclei only one rotational structure has been identified, built on the $\pi h_{11/2} \otimes \nu h_{11/2}$ configuration [5–8]. The lightest odd-odd Cs nucleus with known spectroscopic information is the proton emitter ^{112}Cs [9,10], in which five firm and two tentative transitions have been identified and assigned to the $\pi h_{11/2} \otimes \nu h_{11/2}$ configuration based on systematics [5]. The low-lying states of Cs nuclei have been studied over many years, also exploiting the high yields of radioactive beams of Cs isotopes at ISOL facilities [11,12]. Two long-lived isomers have been identified in ^{118}Cs, the nucleus studied in the present work, one with $T_{1/2} = 14(2)$ s and low spin $I = 2$, and the other with $T_{1/2} = 17(3)$ s and high spin $I = (6, 7, 8)$ [12,13]. The magnetic and spectroscopic quadrupole moments of the long-lived isomers have been measured in an extended range of Cs nuclei, from ^{118}Cs to ^{145}Cs [13], which in many cases led to firm spin and parity assignments, and also to experimentally established deformation of the long-lived isomers on which rotational bands can be built. Nonetheless, the observed band structures in all Cs isotopes and the neighboring

*Present address: Key Laboratory of High Precision Nuclear Spectroscopy and Center for Nuclear Matter Science, Institute of Modern Physics, Chinese Academy of Sciences, Lanzhou 730000, People's Republic of China.

†Deceased.

nuclei have been interpreted by employing calculated deformations, which are significantly smaller, up to 20%–30%, than the measured ones. This induced in some cases difficulties to consistently assign configurations and to reproduce the crossing frequencies of the backbendings observed in the rotational bands. If the adopted deformation is $\varepsilon_2 \approx 0.25$, the $h_{11/2}$ neutrons align first at $\hbar\omega \approx 0.35$ MeV, and the $h_{11/2}$ protons later at $\hbar\omega \approx 0.40$ MeV, see, e.g., the extended TRS calculations in Fig. 8 of Ref. [7]. If, instead, the adopted deformation is $\varepsilon_2 \approx 0.32$, in agreement with the measured spectroscopic quadrupole moments, the opposite is true; that is, the $h_{11/2}$ protons align first at $\hbar\omega \approx 0.35$ MeV, followed by $h_{11/2}$ neutrons which align later at $\hbar\omega \approx 0.40$ MeV (see Sec. III). This ambiguity on the real nuclear deformation highlights the necessity to identify several band structures in a single nucleus, which can help to decide which deformation should be adopted in the calculations. The bands with the unpaired *proton* placed in the $h_{11/2}$ orbital will exhibit $h_{11/2}$ neutron alignments, while the bands with the unpaired *neutron* placed in the $h_{11/2}$ orbital will exhibit $h_{11/2}$ proton alignments at different rotational frequencies. A detailed discussion of the alignment processes in Cs nuclei as arising from total Routhian surface calculations can be found in Ref. [14]. In odd-odd nuclei one can have both types of bands and therefore one can conclude which deformation should be adopted. This is the case in ^{120}Cs [3], in which the band with the unpaired proton in the $\pi g_{9/2}$ orbital exhibits the $h_{11/2}$ proton alignment at $\hbar\omega \approx 0.35$ MeV (Band 3), while the band with the unpaired neutron in the $\nu d_{5/2}$ orbital exhibits the $h_{11/2}$ neutron alignment at $\hbar\omega \geqslant 0.45$ MeV (Band 4).

The calculations of odd-odd nuclei are more demanding because of the multiple band structures resulting from the numerous combinations of the low-lying proton and neutron contributing configurations observed in the adjacent odd-even nuclei, which often lead to isomeric bandheads. Such calculations, employing the configuration-constrained potential-energy-surface (PES) model [15], predict the possible isomeric bandheads in odd-odd lanthanide nuclei [16]. Six to ten isomers are predicted in the light Cs nuclei, with energies up to a few hundreds of keV. Eight isomers have been calculated in ^{118}Cs, with four configurations obtained by coupling a proton in the $d_{5/2}$, $g_{7/2}$, $g_{9/2}$, and $h_{11/2}$ orbitals to a neutron in the $h_{11/2}$ orbital, each one with two possible spin-parity assignments resulting from the Galagher-Moszkowski (GM) coupling rule [17]. If the spins of the two contributing proton and neutron orbitals in the GM doublets are very different, the electromagnetic transitions between the bands based on GM states with low and high spins can be strongly hindered, leading to long-lived isomers, called spin isomers [18], which can decay internally through delayed γ-ray emission or β decay. In all light odd-odd Cs nuclei only one or two long-lived β-decaying isomers are known, with half-lives of several seconds [2]. However, as predicted in Ref. [16], several other isomeric states with possible shorter half-lives can exist and decay internally through γ-ray emission but are not known because no experiments involving suitable setups were performed yet. We therefore undertook a systematic search for low-lying isomers with half-lives measurable using recoil mass spectrometers equipped with efficient detection systems both at the entrance and at the focal plane, with the aim to verify the reliability of the theoretical predictions towards and beyond the proton drip line. Using recoil mass spectrometers one can identify isomers with half-lives of the order or longer than the flight time of the recoils through the spectrometer, usually about a microsecond. Isomers with half-lives between a few hundreds nanoseconds and several tens of microseconds can be identified by means of prompt-delayed coincidences between prompt γ rays emitted by the residual nuclei produced in fusion-evaporation reactions at the target position and delayed γ rays emitted from isomeric states at the focal plane.

Very recently, we have studied the odd-even nuclei ^{119}Cs [19] and ^{119}Ba [20], in which extended sets of single-quasiparticle proton and neutron excitations have been established. In both nuclei we identified low-lying isomers, with half-lives of $T_{1/2} = 0.36(2)$ μs and $T_{1/2} = 55(5)$ μs for the $5/2^-$ and $11/2^-$ bandheads of the bands based on neutron and proton $h_{11/2}$ orbitals in ^{119}Ba and ^{119}Cs, respectively. We were thus in a good position to undertake a study of the odd-odd ^{118}Cs nucleus, in which the low-lying proton-neutron configurations result from the coupling of the single-quasiparticle configurations observed in the adjacent neighbors with an odd number of protons or neutrons. The present work is therefore devoted to the study of the odd-odd nucleus ^{118}Cs, in which the spectroscopic information is limited to only a couple of bands built on top of the 10^+ state [8]. As will be shown in the following, the low-lying band structure of ^{118}Cs is instead very rich.

The presently reported experimental data have been obtained in an experiment performed with the high-efficiency γ-detector array JuroGam 3 [21] and the recoil mass separator MARA [22], using the ^{58}Ni(^{64}Zn, $3pn$)^{118}Cs fusion-evaporation reaction at a beam energy of 255 MeV. Several results obtained from the same experiment have been already published or submitted for publication on ^{119}Cs [19,23,24] and ^{119}Ba [20]. The experimental details are given in Ref. [19] and therefore are not repeated here.

We report ten new bands in ^{118}Cs, as well as other low-lying states, which leads to the largest set of proton-neutron excitations of odd-odd lanthanide nuclei close to the proton drip line. We also report the measured half-life of the bandhead of the $\pi h_{11/2} \otimes \nu h_{11/2}$ band. The configurations of the observed bands are assigned based on the analysis of the alignment properties of the bands, on systematics and particle number conserving cranked shell-model (PNC-CSM) calculations [25,26].

II. EXPERIMENTAL RESULTS

The level scheme of ^{118}Cs divided in two parts is shown in Figs. 1 and 2, and a zoom on the low-lying states is shown in Fig. 3. The complete experimental information on the γ-ray transitions of ^{118}Cs is reported in Table I of the Appendix. Double-gated spectra obtained from prompt $\gamma\gamma\gamma$ coincidences showing the transitions of the newly identified bands reported in the present work are given in Figs. 4–6. Spectra for Bands 1, 6, and 7 obtained from prompt-delayed

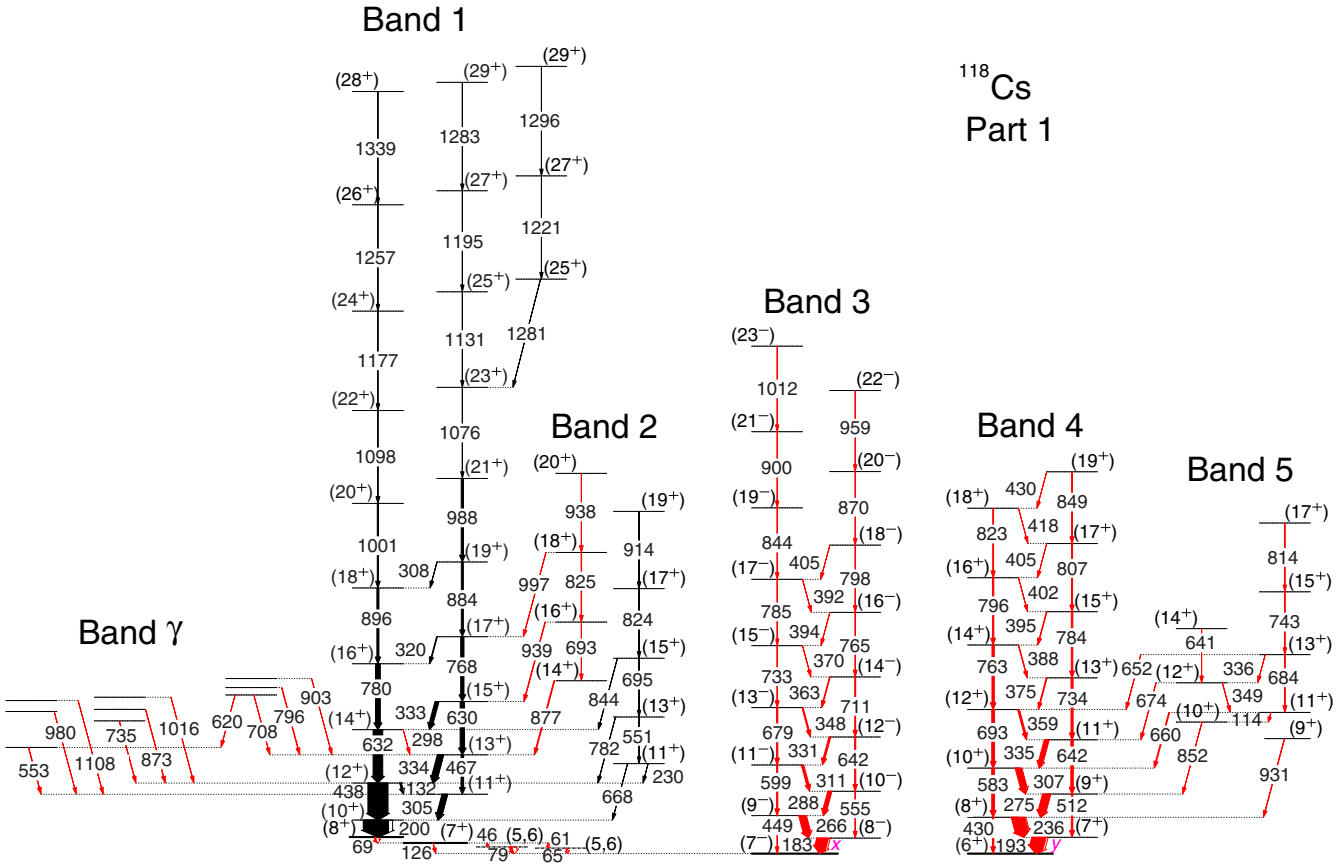

FIG. 1. Part 1 of the level scheme of ^{118}Cs showing the previously known and the presently reported bands. The new transitions are indicated with red color. The isomeric levels are indicated with thick lines. The energies of the bandheads of Bands 3 and 4 are not established experimentally, and therefore are indicated in pink by x and y, respectively.

coincidences of γ rays detected by JuroGam 3 and the detectors at the MARA focal plane are shown in Figs. 7 and 8.

The assignment of the bands to ^{118}Cs is based on the coincidence of the prompt γ-γ coincidences with recoiling evaporation residues with mass 118 detected at the MARA focal plane, and with the 30.8 keV K_α and 35 keV K_β x rays of cesium nuclides detected in prompt coincidence with the in-band transitions by the JuroGam 3 array at the target position. The bands have been established based on coincidence relationships, intensity balance of the states, and, when possible, on the angular correlations of the observed γ rays.

Band 1, first reported in Ref. [8], is the most strongly populated band structure. It is confirmed, except for the highest 1346- and 1408-keV transitions in the two signature partners of the band, which are not observed. The cascade of transitions feeding the state depopulated by the 1076-keV transition is also confirmed. Nine weak transitions feeding the low-lying states of Band 1 up to spin 13^+, and one transition of 620 keV connecting two of them, have been also identified and grouped under the label band γ.

The bandhead spin and parity of Band 1 were first assigned as $I^\pi = 10^+$ in Ref. [8]. However, from the systematics of the $\pi h_{11/2} \otimes \nu h_{11/2}$ bands in odd-odd Cs nuclei published in Ref. [27], it is more likely that the bandhead spin of Band 1 should be 8^+. We therefore adopt spin-parity $I^\pi = 8^+$ for the state populated by the 200-keV transition. We identified a new 69-keV transition which depopulates the 8^+ state, which has an intensity ≈30 times lower than that of the feeding 200-keV transition. The 69-keV transition being weak, we could not extract its electromagnetic character. As the electron conversion coefficients for the possible $E2$, $M1$, or $E1$ electromagnetic characters of the 69-keV transition are 7.0, 2.6, and 0.6, respectively, which cannot account for the missing intensity below the 8^+ state, we can conclude that the 8^+ state is isomeric, with a half-life in the nanosecond range. Unfortunately, we could not measure the half-life of this short-lived isomer, because in the present thin-target experiment the residual nuclei fly away from the focus of the Compton-suppressed γ-ray detectors of the JuroGam 3 array. As the 69-keV transition was not observed at the focal plane in delayed coincidence with Band 1, the half-life of the 8^+ isomer must be much shorter than the flight time of the recoils through the MARA spectrometer, which is of the order of 500 ns. A flight time in the nanosecond range would lead to emission of delayed γ rays at out-of-focus distances in the JuroGam array of the order of centimeters. This would reduce the detection efficiency of the germanium detectors which are equipped with heavy-metal collimators and Compton-suppression shields and can explain the much lower intensity of the delayed 69-keV transition relative to the intensity of

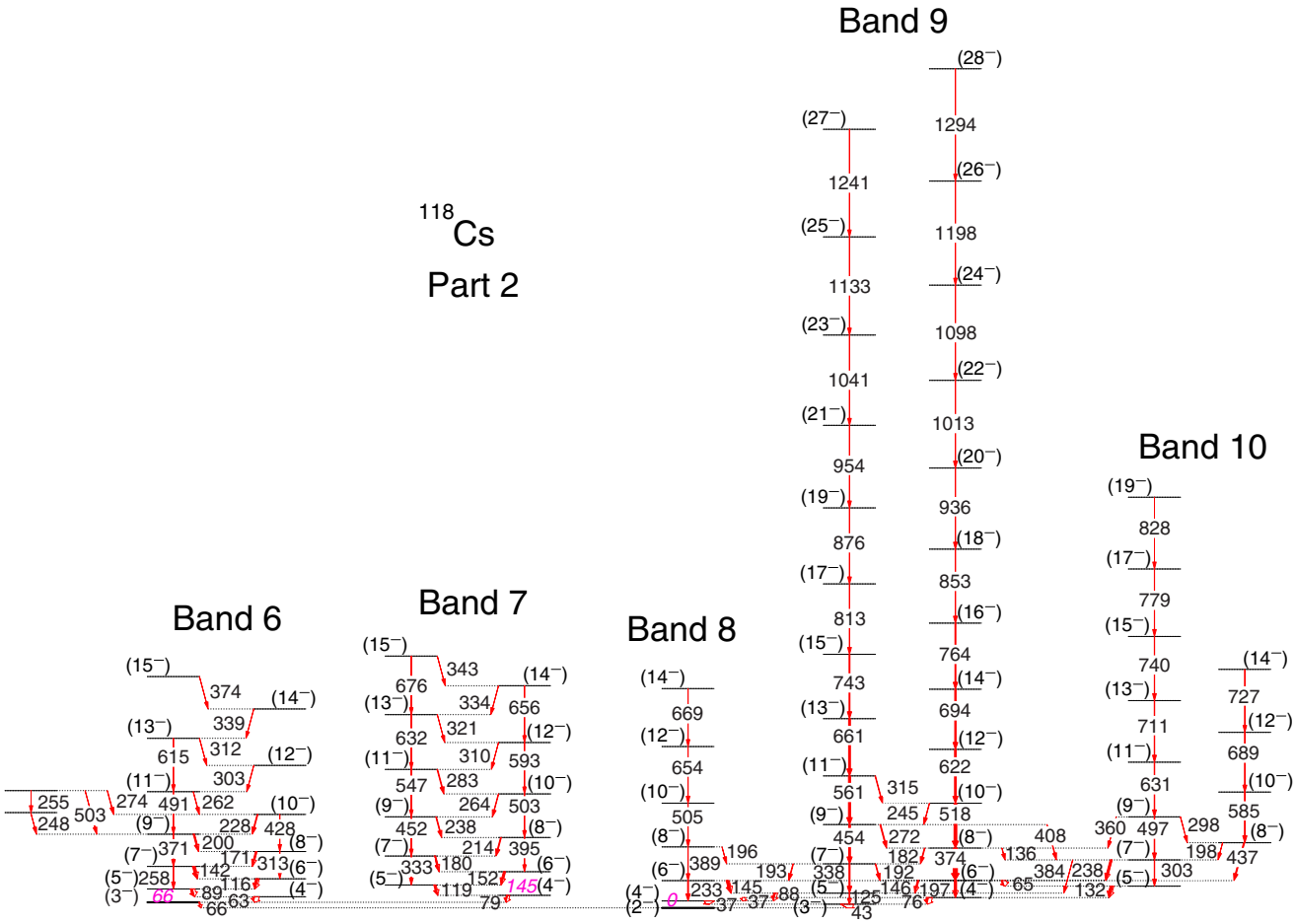

FIG. 2. Part 2 of the level scheme of ^{118}Cs. The new transitions are indicated in red. The isomeric levels are indicated with thick lines. The proposed energies of the bandheads are indicate in pink.

the transitions of Band 1 which are emitted in the focus of JuroGam. The isomeric character of the 8^+ bandhead is similar to that observed for the bandhead of the $\pi h_{11/2} \otimes \nu h_{11/2}$ band in ^{120}Cs, in which the depopulating 183-keV transition measured in a thick-target experiment presented stopped and Doppler-shifted components, indicating an isomeric character with a half-life in the subnanosecond range [3]. Based on the Weisskopf estimates of the transition probability for the 69-keV transition, one can safely exclude the $E1$ and $M2$ characters which lead to long half-lives of 0.85 μs (assuming a hindrance factor of 10^{-6}) and 824 μs, respectively. The half-lives for the $M1$ and $E2$ transitions being $T_{1/2} = 0.06$ ns and $T_{1/2} = 9.8$ μs, respectively, we tentatively assign a mixed $M1 + E2$ character, predominantly $M1$, to the 69-keV transition, leading to a state with $I^\pi = 7^+$. No other transitions in prompt coincidence with the 69-keV transitions have been observed below the 7^+ state.

We then searched for delayed transitions detected at the MARA focal plane in coincidence with the prompt transitions of Band 1 measured at the target position. Five delayed transitions have been identified, with energies of 46, 61, 65, 79, and 126 keV (see Fig. 7), which, based on the prompt coincidence relationships between the HPGe detectors mounted around the MARA focal plane, were placed in three parallel cascades, 46–79, 61–65, and 126 keV, just below the 7^+ state populated by the 69-keV transition. The observation of these delayed γ-ray cascades lead to a state located 126 keV below the 7^+ isomer, to which we tentatively assigned spins and parities based on the analysis of the isomer decay, as described in the following. No other transitions have been observed at the MARA focal plane in coincidence with the delayed transitions depopulating the 7^+ isomer, indicating that the three γ-ray branches populate one of the two known long-lived isomers, which can only be the $I = (6, 7, 8)$, $T_{1/2} = 17(3)$ s isomer [12], since the observed delayed transitions depopulate the high-spin 7^+ state and cannot have the high multipolarity required to populate the $I = 2$ isomer [11]. A half-life $T_{1/2} = 0.55(6)$ μs has been extracted from the fit of the time spectrum obtained by summing the time spectra of the 79- and 126-keV depopulating transitions of the 7^+ isomer, as shown in Fig. 9. As we could not perform an angular-correlation analysis of the events measured at the MARA focal plane, the electromagnetic characters of these transitions are not established experimentally. The half-life of the 7^+ isomer can be accounted for by assuming $E1$, $E2$, or $M2$ electromagnetic characters of the 126-keV transition, which lead to spins and

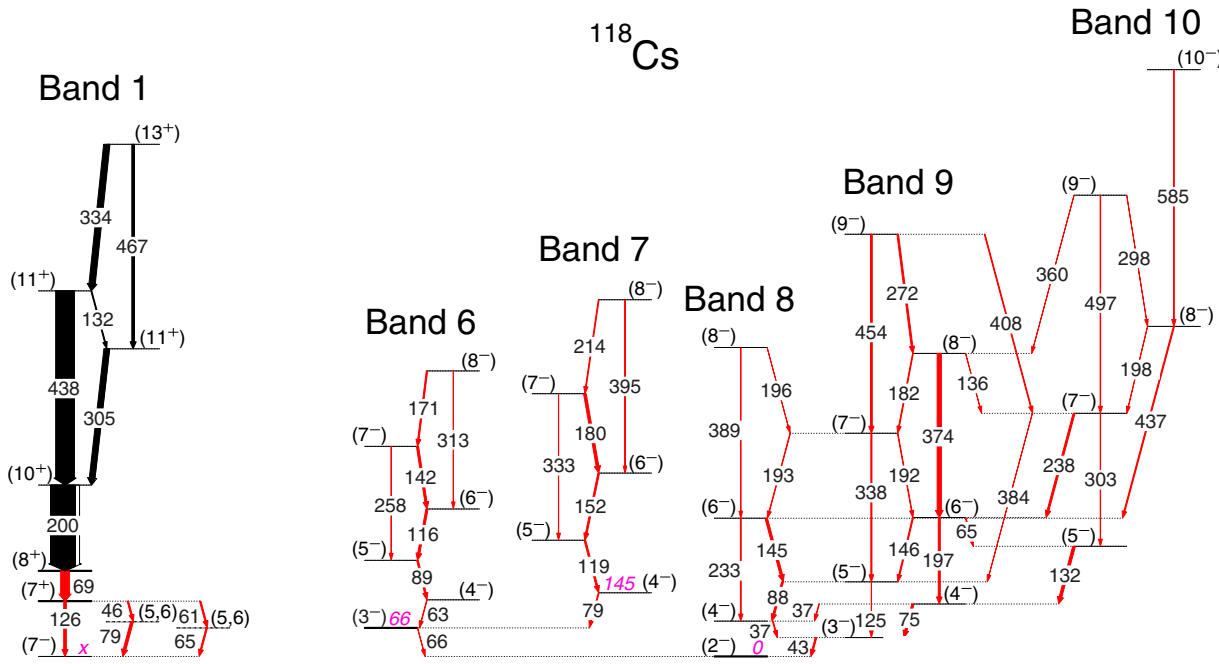

FIG. 3. Zoom on the low-lying states of the level schemes of ^{118}Cs shown in Figs. 1 and 2. The proposed energies of the bandheads are indicated in pink.

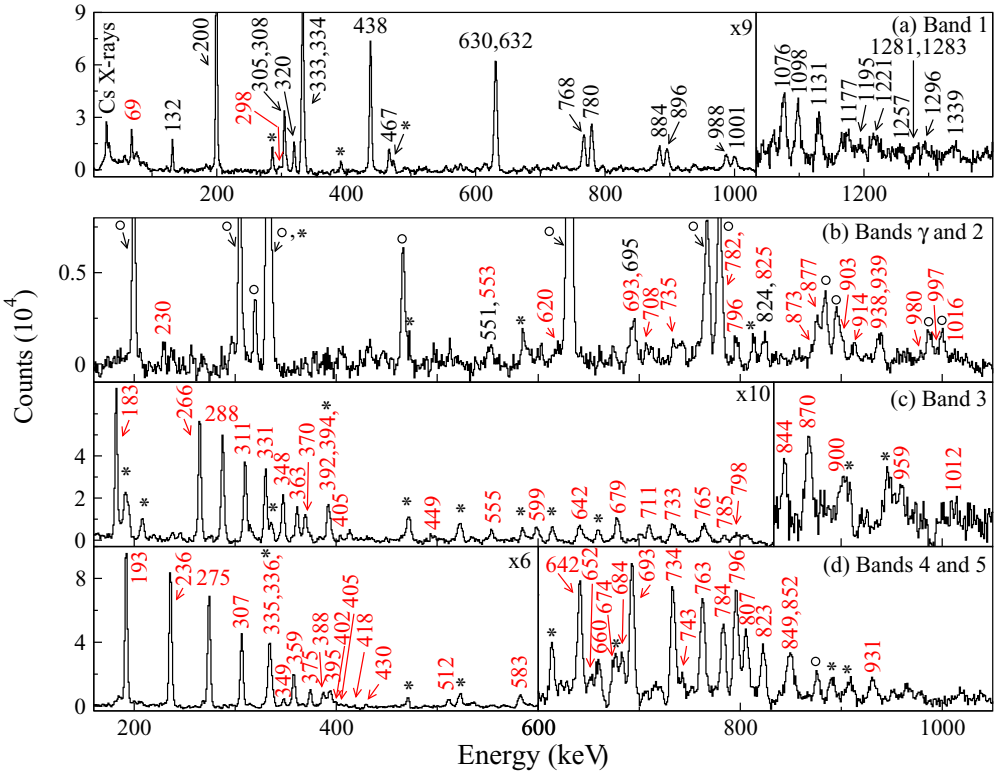

FIG. 4. Double-gated spectra for Bands 1, γ, 2, 3, 4, and 5 of ^{118}Cs. Peak energies for the newly identified bands are written in red. Transitions from other nuclei are indicated with an asterisk, while those from Band 1 present in the spectrum of band 2 ^{118}Cs are indicated with a circle. The lists of gating transitions for each spectrum are the following: for Band 1: 132, 200, 305, 438, 467, 632, 768, 780, 884, 896, 988, 1001, 1077, 1098, 1176, 1339 keV; for Bands 2 and γ: 132, 200, 305, 334, 438, 467 keV; for Band 3: 183, 266, 288, 311, 331, 348, 363, 555, 599, 642, 679 keV; for Bands 4 and 5: 193, 236, 275, 307, 388, 512, 583, 642, 693, 734, 763 keV.

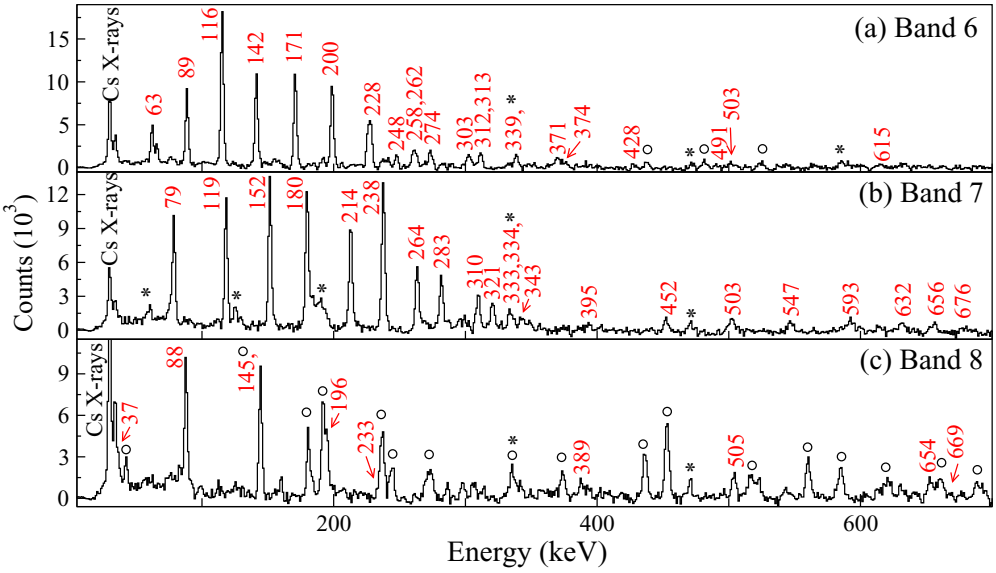

FIG. 5. Double-gated spectra for Bands 6–8 of ^{118}Cs. Peak energies for the newly identified bands are written in red. Transitions from other nuclei are indicated with an asterisk, while those from other bands in ^{118}Cs are indicated with a circle. The lists of gating transitions for each spectrum are the following: for Band 6: 89, 142, 171, 200, 228 keV; for Band 7: 79, 119, 152, 180, 214, 264 keV; for Band 8: 88, 145, 193, 389, 505, 654 keV.

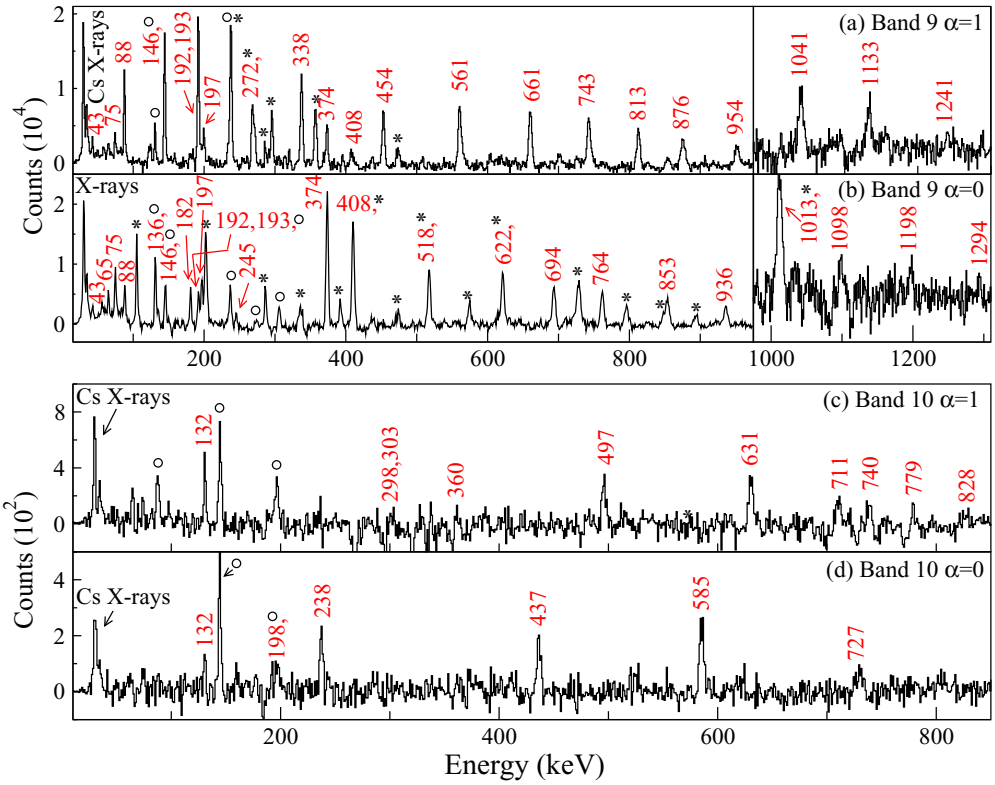

FIG. 6. Double-gated spectra for Bands 9 and 10 of ^{118}Cs. Peak energies for the newly identified are written in red. Transitions from other nuclei are indicated with an asterisk, while those from other bands in ^{118}Cs are indicated with a circle. The lists of gating transitions for each spectrum are the following: Band 9 ($\alpha = 0$): 197, 518, 622, 694, 764, 853, 936, 1013, 1098 keV; Band 9 ($\alpha = 1$): 88, 454, 561, 661, 743, 813, 876, 954, 1041 keV; Band 10 ($\alpha = 0$): sum of double gates 88/689 + 198/689 keV; Band 10 ($\alpha = 1$): sum of double gates 631/711 + 631/740 + 711/740 + 238/711 + 238/497 + 132/711 keV.

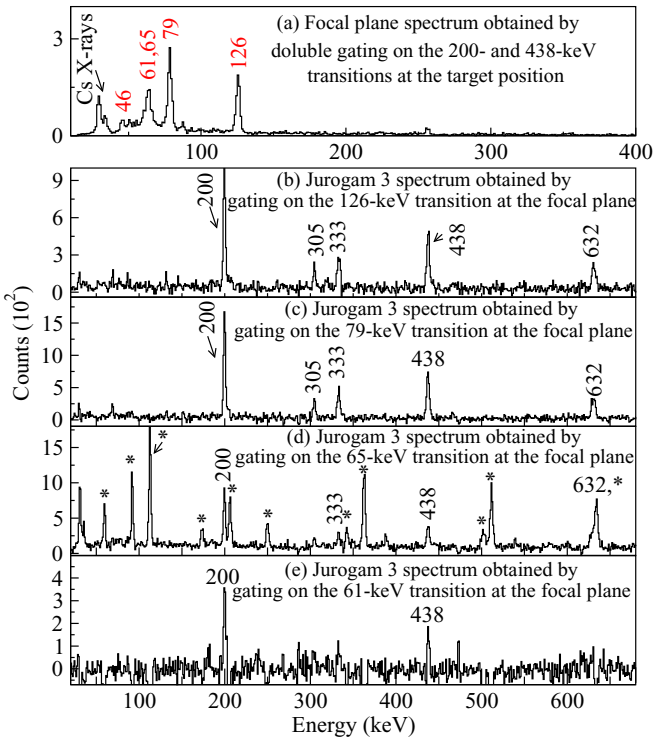

FIG. 7. Prompt-delayed coincidence spectra for Band 1. Peak energies for the newly identified transitions are in red. The asterisks in panel (d) indicate transitions of Band 1 in ^{119}Ba [20].

parities between 5^+ and 8^- for the state fed by the 126-keV transition. Taking also into account the prompt coincidence between the 46- and 79-keV transitions and between the 61- and 65-keV transitions, only states with spins and parities 6^- and 7^- for the final state can lead to an isomer half-life in the microsecond range.

As will be discussed in the following, based on the Gallagher-Moszkovski coupling rule (GM) [17], high-spin isomers with $I^\pi = 7^-$ and 6^+ in ^{118}Cs can arise from one proton in the $\pi g_{9/2}[404]9/2^+$ orbital observed at 86 keV in ^{119}Cs, and from a neutron in the $\nu h_{11/2}[532]5/2^-$ or $\nu d_{5/2}[411]3/2^+$ orbitals observed at 66 and 53 keV in ^{119}Ba, respectively. As will be discussed in the following, we assigned spin-parity 7^- to Band 3, and therefore we identified the long-lived isomeric

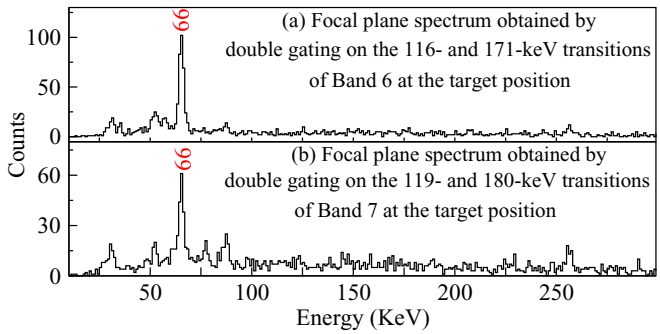

FIG. 8. Prompt-delayed coincidence spectra for Bands 6 and 7. Peak energies for the newly identified transitions are in red.

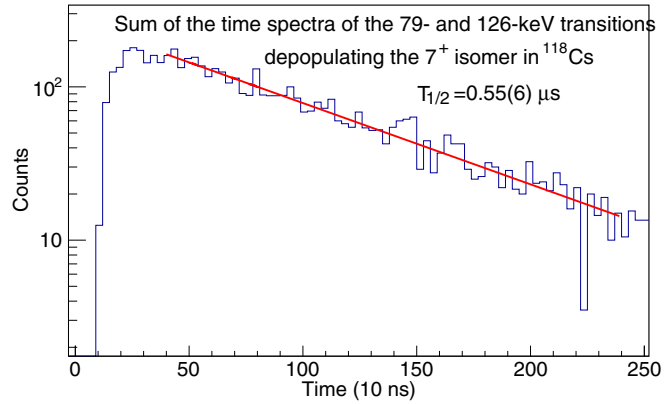

FIG. 9. Fit of the time spectrum obtained by summing the time spectra of the 79- and 126-keV transitions depopulating the 126-keV 7^+ isomer of ^{118}Cs, produced by gating on the 200-keV transition detected with JuroGam 3 at the target position.

state populated by the 126-keV transition with the 7^- bandhead of Band 3.

The order of the transitions in the two 46–79 keV and 61–65 keV cascades, as well as the spins and parities of the intermediate levels in these cascades, could not be established, because many combinations of spins and parities lead to half-lives of the order of a microsecond for the 7^+ isomer. Therefore, the intermediate levels in these cascades have spins 5 or 6, and their excitation energies and parities are not fixed (see Figs. 1 and 3).

Band 2 is very weakly populated and is composed of two cascades of $E2$ transitions feeding states of Band 1 up to spins 17^+. The odd-spin cascade of Band 2 up to spin 19 and its connecting transitions to Band 1 have been previously reported in Ref. [8], but were wrongly placed to feed states of the odd-spin cascade of Band 1. The even-spin cascade is newly identified. No transitions between the odd- and even-spin cascades are observed. The coincidence relationships of the present work clearly show that the 668-keV transition, the 230- and 782-keV transitions, and the weak 844-keV transition directly populate the even-spin states 10^+, 12^+, and 14^+ of Band 1, respectively. The spins and positive-parity are tentative, being based on their alignment properties and PNC-CSM calculations.

Band 3 is newly identified. It is populated with an intensity ≈50% of that of Band 1 and is composed of two long cascades of $E2$ transitions up to spin 23, interconnected by strong $M1 + E2$ transitions up to spin 18. We tentatively assign a spin-parity 7^- to the bandhead, based on the intensity of the band, on systematics and on the PNC-CSM calculations (see the discussion section). No other prompt transitions depopulating the 7^- bandhead at the target position, or delayed transitions detected at the MARA focal plane in coincidence with in-band transitions detected at the target position, have been observed. This indicates the isomeric character of the 7^- bandhead, with a half-life of at least several microseconds. We identify the bandhead of Band 3 with the $T_{1/2} = 17(3)$ s isomer for which a spin $I = (6, 7, 8)$ has been suggested [12], selecting thus $I = 7$ among the three possible spin values, and

we assign it negative parity, leading therefore to $I^\pi = 7^-$ for the $T_{1/2} = 17(3)$ s isomer.

Band 4 is newly identified. It is populated with an intensity ≈50% of that of Band 1. It is composed of two cascades of $E2$ transitions, interconnected by strong $M1 + E2$ transitions up to spin 19. Even if Band 4 has properties similar to those of Band 3, no transitions have been observed between the two bands, suggesting opposite parities. We can tentatively assign $I^\pi = 6^+$ for the bandhead, which is in agreement with the $\pi[404]9/2^+ \otimes \nu[411]3/2^+$ favored configuration predicted by the GM rule. An alternative configuration can be $\pi[404]9/2^+ \otimes \nu[413]5/2^+$, which leads to $I^\pi = 4^+$ for the bandhead (see the discussion section). No other transitions have been observed at the target position in prompt coincidence with in-band transitions, indicating an isomeric character of the bandhead with a half-life of at least several microseconds, as in the case of Band 3. A weakly populated band, labeled Band 5, feeding the states of Band 4 with spins between 8^+ and 12^+ has also been identified.

Band 6 is newly identified. It has an intensity of ≈15% of that of Band 1. It is composed of strong $M1 + E2$ transitions, and weak $E2$ crossover transitions. No other prompt transitions detected at the target position were observed in coincidence with the strong $M1 + E2$ in-band transitions, but a delayed 66-keV transition has been observed at the MARA focal plane in coincidence with the in-band transitions observed at the target position. As the 66-keV transition is also observed in coincidence with the in-band transitions of Band 7, we placed it on top of the ground state to which we assigned spin-parity $I^\pi = 2^-$ (see the following discussion). Based on the PNC-CSM calculations which suggest a $\pi[541]3/2^- \otimes \nu[411]3/2^+$ configuration for Band 6, we tentatively assign $I^\pi = 3^-$ to its bandhead. With this assignment, the isomeric character of the $I^\pi = 3^-$ bandhead of Band 6 at an excitation energy of 66 keV is induced by a hindrance due to the very different configuration to the $\pi[404]9/2^+ \otimes \nu[532]5/2^-$ configuration assigned to the ground state (see the discussion section). Due to insufficient statistics, the half-life of the 66-keV isomeric state could not be measured from the delayed spectra collected at the MARA focal plane.

Band 7 is newly identified. It is populated with an intensity of ≈10% of that of Band 1 and is composed of levels connected by strong $M1 + E2$ transitions and a few weak $E2$ crossover transitions. No other prompt transitions detected at the target position were observed in coincidence with in-band transitions, but, as in the case of Band 3, a delayed 66-keV transition has been observed at the MARA focal plane in coincidence with the in-band transitions observed at the target position. We assumed that this delayed transition is the same as that observed in delayed coincidence with Band 6, and we placed the lowest prompt 79-keV transition on top of the 66-keV state, which leads to spin-parity 4^- for the bandhead of Band 7. The assigned $\pi[422]3/2^+ \otimes \nu[532]5/2^-$ configuration being very different from that assigned to Band 6 explains the missing connecting transitions between the two bands.

Five cascades of $E2$ transitions interconnected by many $M1 + E2$ and three $E2$ transitions, which were grouped in three bands with labels 8, 9, and 10, are newly identified, being populated with intensities of 45%, 60%, and 15% of that of Band 1, respectively (see Figs. 2 and 3). The many low-energy interconnecting transitions have most probably mixed $M1 + E2$ character, leading to identical parity of all five $E2$ cascades, which we assign as negative. The lowest state of these negative-parity bands is that populated by the 43-keV transition from Band 9. Based on the systematics of the spins and parities of the low-lying bands in the neighboring odd-odd iodine nuclei [28], and on the existence of a long-lived $T_{1/2} = 14(2)$ s, $I = 2$ isomer [12], we assign spin-parity 2^- to this state, which we assign as the bandhead of Band 8 and adopt as the ground state of ^{118}Cs.

Band 9 is composed of two long cascades of $E2$ transitions developing up to spin 28^-, interconnected by $M1 + E2$ transitions up to spin 11^-. Seven connecting transitions have been identified between Band 8 and Band 9. The odd-spin cascade of Band 9 is connected by the 408- and 384-keV transitions to Band 10, linking states with possible difference in spin of $2\hbar$, and therefore having $E2$ character. This would imply that both bands have the same parity, which we assigned as negative parity. The 8^- state of Band 10 mainly decays to Band 8, while the two 198- and 298-keV transitions interconnect the odd- and even-spin states of the band.

III. DISCUSSION

A. General considerations

The structure of the odd-odd nucleus ^{118}Cs is more complex than that of the odd-even neighboring nuclei ^{119}Cs and ^{119}Ba, on which detailed experimental information and theoretical interpretations have been reported very recently [19,20,23,24]. Its discussion should start from the two known long-lived isomers, for which, however, the excitation energies and parities have not been experimentally established [12,13]. The last NNDC evaluation of ^{118}Cs has been released long time ago, in 1995 [2], and consists of only one band, which was in fact wrongly assigned to ^{118}Cs [29]. This wrong assignment of a band of ^{118}I to ^{118}Cs has been already mentioned in Ref. [8], but not yet corrected on the ENSDF website.

As the excitation energies relative to the ground states of the observed bands in ^{119}Cs and ^{119}Ba lie within 200 keV, the expected excitation energies of the bands in ^{118}Cs are also expected to be low, lying within a few hundreds of keV. This expectation is also supported by the theoretical predictions of Ref. [16], in which the energies of the four low-lying isomers are calculated between zero and 161 keV. However, as discussed above, not all bands observed in ^{118}Cs could be interconnected by γ-ray transitions, as in the case of the neighboring ^{119}Cs and ^{119}Ba [19,20], and therefore their relative excitation energies could not be established. This uncertainty also induces an inherent difficulty in the assignment of spins and parities to the observed bands. In the following discussion we will only tentatively assign spin parities and excitation energies to the observed bands.

The present complex level scheme of ^{118}Cs can be viewed as consisting of several groups of bands. The first group consists of the strongly populated positive-parity Band 1 and

the weakly populated bands and states decaying to it. It is built on top of the high-spin 7^+ isomer with a half-life $T_{1/2} = 0.55(6)$ μs, which we assume to decay through several transitions to the long-lived 7^-, $T_{1/2} = 17(3)$ s isomer, assigned as bandhead of Band 3. The second group consists of the well-populated strongly coupled Bands 3 and 4 composed of long cascades of strong dipole and crossover $E2$ transitions, and the weakly populated Band 5 which decays to Band 4. As no delayed transitions have been observed despite the strong population of these bands, one can conclude that they are built on long-lived isomers, which can occur if the bands have low excitation energies, and/or have spin-parity that hinder their decay to low-spin states. To account for the missing interconnecting transitions between Bands 3 and 4, we assigned them opposite parities, negative to Band 3 and positive to Band 4, and bandhead spin-parity 7^- and $(6^+, 4^+)$, respectively. The third group consists of Bands 6 and 7, which are composed of shorter sequences of dipole transitions than Bands 3 and 4, and weak crossover transitions. They decay via the delayed 66-keV transition that we placed above the assigned 2^- ground state, leading to spins and parities 3^- and 4^- for the bandheads of Bands 6 and 7, respectively. The fourth group consists of Bands 8–10, which are interconnected by many transitions, and we place on top of the 2^- ground state. Therefore, these three bands have all tentatively assigned negative parity.

The spin assignment to the 8^+ bandhead of the $\pi h_{11/2} \otimes \nu h_{11/2}$ band, which in ^{118}Cs is Band 1, was done based on systematics [27]. An alternative 10^+ assignment can result from the comparison with the reported level scheme of the neighboring ^{120}Cs nucleus [4]. However, this alternative assignment is not supported by the present results, which reveal the existence of a 69-keV $M1$ transition depopulating the bandhead of Band 1, in cascade with a delayed 126-keV $E1$ transition, leading to a long-lived isomer with an excitation energy of 196 keV lower than that of the bandhead, to which we assign spin-parity 7^-. A 10^+ assignment to the bandhead of Band 1 would lead to a $I^\pi = 9^-$ isomer, which does not correspond to any possible low-lying two-quasiparticle configuration, and also was not observed in any neighboring nucleus. We therefore propose the $I^\pi = 7^-$ assignment to the state populated by the 126-keV transition, which we identify with the $T_{1/2} = 17(3)$ s isomer and we assign to the bandhead of Band 3. This assignment gives therefore support to the $I = 8^+$ spin-parity for the bandhead of Band 1.

The spins and parities of the other bands are based on the following alignment analysis and PNC-CSM calculations and are therefore tentative.

B. Alignment analysis and configuration assignments

Single-particle angular momenta i_x as a function of the rotational frequency $\hbar\omega$ are shown in Fig. 10. One can see that all bands except Bands 1 and 2 exhibit i_x values below $\approx 3.5\hbar$ at low rotational frequencies and alignment gains at rotational frequencies of $\hbar\omega \leqslant 0.35$ MeV. It results that in all bands except in Bands 1 and 2, at most one proton or one neutron occupies an $h_{11/2}$ orbital, leaving thus unblocked the $h_{11/2}$ alignment of one proton, of one neutron, or of both

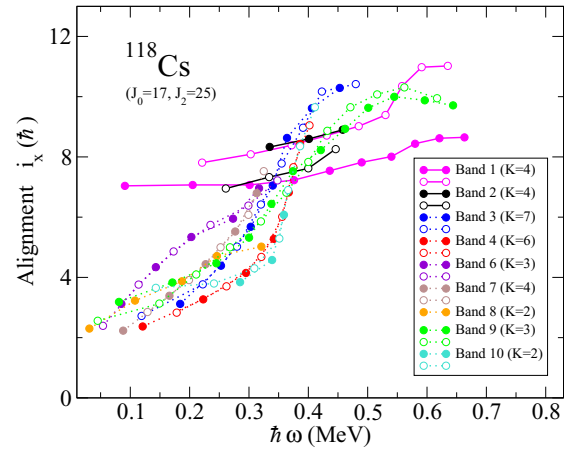

FIG. 10. Single-particle angular momenta i_x of all bands of ^{118}Cs. The Harris parameters are $J_0 = 17\,\hbar^2$ MeV^{-1} and $J_0 = 25\,\hbar^4$ MeV^{-3}. The K values corresponding to the adopted bandheads of each band are also indicated. The states with signature $\alpha = +1/2$ and $\alpha = -1/2$ are drawn with filled and open symbols, respectively. The positive-parity and negative-parity bands are drawn with continuous and dotted lines, respectively.

of them. The first alignment gains at $\hbar\omega \approx 0.4$ MeV can be induced by either $h_{11/2}$ protons or $h_{11/2}$ neutrons, depending on the deformation: for $\varepsilon_2 \approx 0.3$ the $h_{11/2}$ protons align first at $\hbar\omega \approx 0.35$ MeV, followed by $h_{11/2}$ neutrons which align at $\hbar\omega \approx 0.45$ MeV, whereas for a smaller deformation of $\varepsilon_2 \approx 0.25$ the opposite occurs, that is the $h_{11/2}$ neutrons align before the $h_{11/2}$ protons.

The alignment exhibited in Band 1 is around $7\hbar$, in agreement with the $\pi[541]3/2^- \otimes \nu[532]5/2^-$ configuration previously assigned in Ref. [8]. It does not show any alignment gain up to a rotational frequency of $\hbar\omega \approx 0.5$ MeV, indicating the blocking of both the $h_{11/2}$ proton and neutron alignments, and therefore indicating a configuration with the unpaired proton and unpaired neutron placed in the $h_{11/2}$ orbitals. The alignment increases gradually up to $\hbar\omega \approx 0.5$ MeV, where gains of $\approx 2\hbar$ and $\approx 1\hbar$ in the $\alpha = 1$ and $\alpha = 0$ signature partners, respectively, are exhibited. These alignment gains have been attributed to $h_{11/2}$ neutrons in Ref. [8], but as discussed in the following section, the present calculations suggest that should be attributed to $h_{11/2}$ protons (see Fig. 13).

The alignments exhibited by the two signature partners of Band 2 are very similar to those of Band 1, suggesting a configuration similar to that of Band 1, that is, $\pi[541]3/2^- \otimes \nu[532]5/2^-$.

The alignment of Band 3 is around $2.5\hbar$ at low frequency, exhibits an alignment gain of $\approx 8\hbar$ at $\hbar\omega \approx 0.35$ MeV, and saturates at $i_x \approx 10\hbar$ at high frequency. This alignment pattern indicates the blocking of a second $h_{11/2}$ alignment, and therefore excludes a configuration involving two positive-parity orbitals. It is very similar to that of Band 8 of ^{119}Cs, which has an excitation energy of 86 keV and $\pi g_{9/2}[404]9/2^+$ configuration [24], suggesting therefore the presence of the $\pi g_{9/2}[404]9/2^+$ proton orbital in its configuration, and thus keeping free the $\pi h_{11/2}$ proton orbital which induces the

observed alignment gain. The unpaired neutron should be placed in the lowest negative-parity orbital $\nu h_{11/2}[532]5/2^-$, which generates Band 1 in the neighboring odd-even ^{119}Ba nucleus at an excitation energy of 66 keV [20]. The coupling of these two orbitals leads to the $\pi g_{9/2}[404]9/2^+ \otimes \nu h_{11/2}[532]5/2^-$ configuration, which is expected to have a low excitation energy. We therefore assign the $\pi g_{9/2}[404]9/2^+ \otimes \nu h_{11/2}[532]5/2^-$ configuration to Band 3. The small alignment at low frequency of $i_x \approx 2.5\hbar$ is in agreement with the assigned configuration, since only the $\nu h_{11/2}[532]5/2^-$ neutron in the $h_{11/2}$ midshell orbital contributes to the alignment, the strongly coupled $\pi g_{9/2}[404]9/2^+$ proton having negligible alignment. As the $\nu[532]5/2^-$ orbital is occupied, the $h_{11/2}$ neutron alignment is blocked, and the alignment observed at $\hbar\omega \approx 0.3$ MeV is therefore due to a pair of $h_{11/2}$ protons.

The alignment exhibited by Band 4 is similar to that of Band 3 but occurs at a slightly higher frequency of $\hbar\omega \approx 0.35$ MeV. Despite the very similar alignment patterns, Bands 3 and 4 are not connected by any transition, indicating very different configurations. This can occur if the unpaired proton is in the same high-Ω positive-parity $\pi g_{9/2}[404]9/2^+$ orbital as in Band 3, while the neutron is instead in a positive-parity orbital, leading to positive parity for Band 4, therefore opposite to that of Band 3, and leading to $E1$ or $M2$ connecting transitions that are hindered. The best agreement of the moment of inertia is obtained by involving the $\nu g_{7/2}[411]3/2^+$ orbital. The configuration of Band 4 can therefore be $\pi g_{9/2}[404]9/2^+ \otimes \nu g_{7/2}[411]3/2^+$, leading to a bandhead of $I^\pi = 6^+$. With this assignment both the $h_{11/2}$ proton and $h_{11/2}$ neutron alignments are not blocked. An alternative configuration could be $\pi g_{9/2}[422]3/2^+ \otimes \nu d_{5/2}[413]5/2^+$, which leads to bandhead spin 4^+. This alternative configuration having both the proton and neutron orbitals different from those of Band 3, can also account for the missing connecting transitions between Bands 3 and 4.

Bands 6 and 7 exhibiting smooth up-bends with steeper slopes than in the other bands. They are composed of degenerate signature partners and are not connected by any transition. The near degeneracy of the signature partners in both bands strongly suggests the occupation of high-Ω orbitals. Possible configurations have been investigated, and the best agreements have been obtained for the $\pi[541]3/2^- \otimes \nu[411]3/2^+$ for Band 6 leading to bandhead spin-parity 3^-, and $\pi[422]3/2^+ \otimes \nu[532]5/2^-$ for Band 7 leading to bandhead spin-parity 4^-.

Bands 8–10 are interconnected by several transitions, leading to the same parity for all three bands, which we assigned as negative. The alignment exhibited by Bands 8 and 9 are similar but more gradual than those of Bands 3 and 4. An alignment gain of $\approx 7\hbar$ at $\hbar\omega \approx 0.35$ MeV is exhibited, which saturates at high frequency at $i_x \approx 10\hbar$, like in Band 3, and therefore should be due to the alignment of $h_{11/2}$ protons. There are two positive-parity proton orbitals, $\pi[420]1/2^+$ and $\pi[422]3/2^+$, that can be coupled with a neutron in the $\nu[532]5/2^-$ orbital to give rise to possible configurations for Bands 8–10, which are $\pi[420]1/2^+ \otimes \nu[532]5/2^-$ and $\pi[422]3/2^+ \otimes \nu[532]5/2^-$, with favored (unfavored) bandhead spins given by the GM rule as $3^-(2^-)$ and $1^-(4^-)$, respectively.

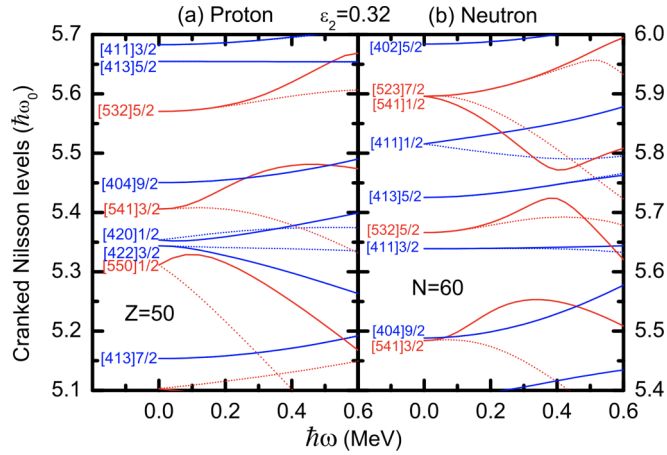

FIG. 11. Single-particle Routhians located in the vicinity of the Fermi level of the ^{118}Cs as a function of rotational frequency for axial prolate deformation of $\varepsilon_2 = 0.32$: (a) protons and (b) neutrons. Positive (negative) parity Routhians are shown by blue (red) lines. Solid (dotted) lines are used for signature $\alpha = +1/2$ ($\alpha = +1/2$).

Bands 8 and 9 being connected by strong transitions and having a similar alignment, can be based on the GM partners of the same $\pi[420]1/2^+ \otimes \nu[532]5/2^-$ configuration, with $K = 2$ and $K = 3$, respectively. Band 10 can have the same $\nu[422]3/2^+ \otimes \nu[532]5/2^-$ configuration as Band 7, but built on $K = 1$ GM partner, which is in agreement with its lower alignment than that of Band 7.

C. Particle number conserving cranked shell-model calculations

To investigate the possible configurations of the observed bands we performed PNC-CSM calculations, in which the phenomenological Nilsson potential is adopted for the mean field [25], with parameters κ and μ taken from Ref. [30] and effective monopole pairing strengths of 0.8 MeV for protons and 0.6 MeV for neutrons. This model was recently used to successfully describe the band structure in rare-earth nuclei [26]. In the present work we do not discuss the γ band which cannot be described by the PNC-CSM calculations, and the very weakly populated Band 5 which has tentative spins and parity assignments. Single-particle Routhian diagrams as function of rotational frequency for prolate deformation are shown in Fig. 11. They were used to guide the search for the quasiparticle orbitals closest to the proton and neutron Fermi surfaces.

The moments of inertia for similar bands observed in ^{118}Cs and ^{120}Cs [3] are shown for comparison in Fig. 12. One can see bands with very similar pattern in both nuclei, which indicate similar configurations. In ^{118}Cs we identified two more bands than in ^{120}Cs, which are Bands 4 and 6. Bands with similar patterns are also known in ^{116}I [31], but we did not include them in the figure which would become too difficult to read.

We performed PNC-CSM calculations for all configurations involving proton and neutron orbitals close to the Fermi

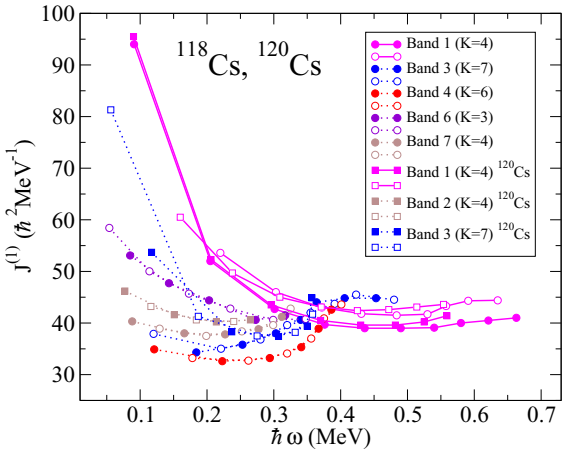

FIG. 12. Moments of inertia $J^{(1)}$ of all bands of ^{118}Cs and of ^{120}Cs [3]. The states with signature $\alpha = +1/2$ and $\alpha = -1/2$ are drawn with filled and open symbols, respectively.

surfaces. In the configuration assignment process we took into account the alignment properties discussed in the preceding section, the relative intensities and decay properties of the bands, as well as the systematics of both odd-even and odd-odd nuclei in the region. Of considerable help were our recent works on ^{119}Cs and ^{119}Ba [19,20], in which we assigned configurations to all low-lying bands based on similar calculations. We adopted an axial deformation with $\varepsilon_2 = 0.32$, similar to that used for ^{119}Cs and ^{119}Ba. The results are presented in Figs. 13–18.

One can see that Bands 1 and 2 are well reproduced by the same $\pi[541]3/2^- \otimes \nu[532]5/2^-$ configuration, involving the $\alpha = -1/2$ and $\alpha = +1/2$ signature partners of the $\pi[541]3/2^-$ orbital in Band 1 and Band 2, respectively. The first proton and neutron $h_{11/2}$ alignments being blocked, the calculated J_x increases smoothly up to high frequencies of $\hbar\omega \approx 0.6$ MeV, where the second proton and second neutron alignments occur. The calculated spin aligned along the rotation axis J_x for Band 2 is slightly lower than that of Band 1, which is in disagreement with the experiment, pointing to a slightly smaller deformation of Band 2, like in the case of Band 2 of ^{119}Cs which is built on the $\pi[541]3/2^-(\alpha = -1/2)$ orbital [19].

The configurations assigned to Bands 3 and 4 are based on their alignment pattern, which is similar to that of the Band 8 of ^{119}Cs which is built on the $\pi[404]9/2^+$ orbital [19]. It is well reproduced over the entire observed frequency range, while the increase of the moment of inertia at $\hbar\omega \approx 0.35$ MeV is calculated to be a bit more rapid than the observed one. The configuration assigned to Band 4 involves the same $\pi[404]9/2^+$ proton orbital as in Band 3, which can be coupled to either the $\nu[411]3/2^+$ or $\nu[413]5/2^+$ positive-parity neutron orbitals to obtain the observed increase of the moment of inertia at $\hbar\omega \approx 0.35$ MeV. The alignment gain is equally well reproduced by the two alternative configurations, being induced by $h_{11/2}$ protons. The coupling with the $\nu[413]5/2^+$ orbital reproduces better the observed pattern. However, we prefer to assign the $\pi[404]9/2^+ \otimes \nu[411]3/2^+$ configuration to Band 4, because the present PNC-CSM calculations

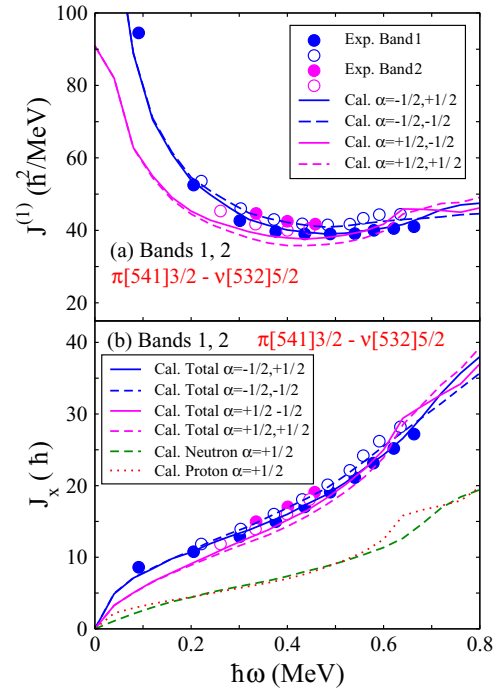

FIG. 13. (a) Moment of inertia $J^{(1)}$, (b) projection of the angular momentum on the cranking axis J_x for the $\pi[541]3/2^-(\alpha = -1/2) \otimes \nu[532]5/2^-$ configuration assigned to Bands 1 and 2 of ^{118}Cs based on the PNC-CSM calculations for a deformation of $\varepsilon_2 = 0.32$. The states with signature $\alpha = +1/2$ and $\alpha = -1/2$ are drawn with filled and open symbols, respectively. The signatures of the proton and neutron orbitals involved in each configuration are also indicated.

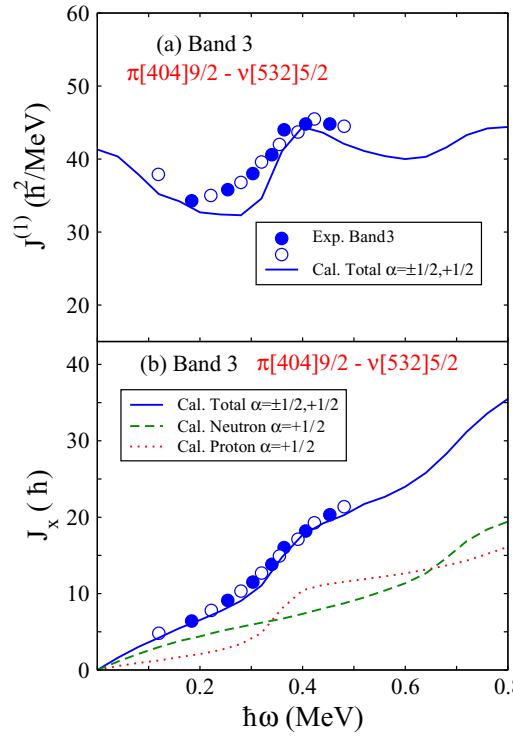

FIG. 14. The same as in Fig. 13 for Band 3, for the configuration $\pi[404]9/2^+ \otimes \nu[532]5/2^-$.

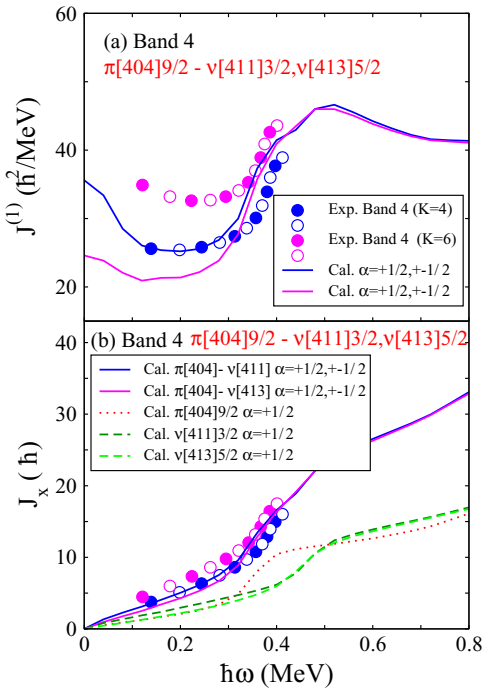

FIG. 15. The same as in Fig. 13 for Band 4, for the configurations $\pi[404]9/2^+ \otimes \nu[411]3/2^+$ and $\pi[404]9/2^+ \otimes \nu[413]5/2^+$.

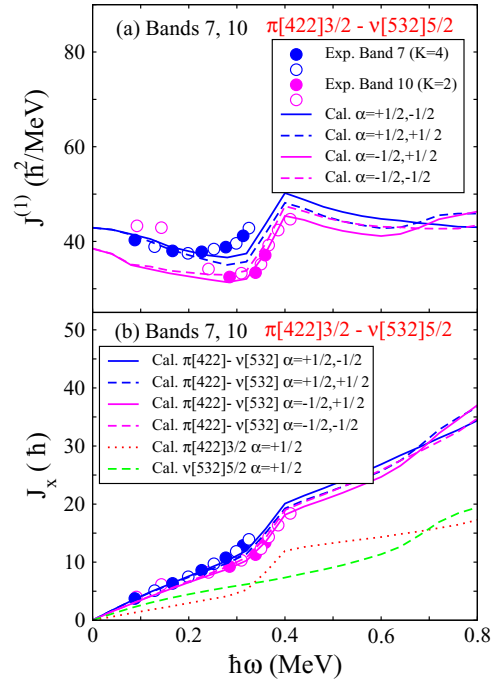

FIG. 17. The same as in Fig. 13 for Bands 7 and 10, for the configuration $\pi[422]3/2^+ \otimes \nu[532]5/2^-$.

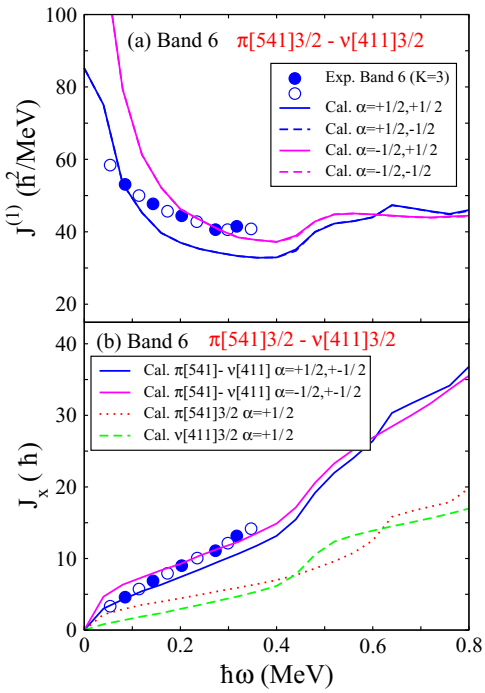

FIG. 16. The same as in Fig. 13 for Band 6, for the configuration $\pi[541]3/2^- \otimes \nu[411]3/2^+$.

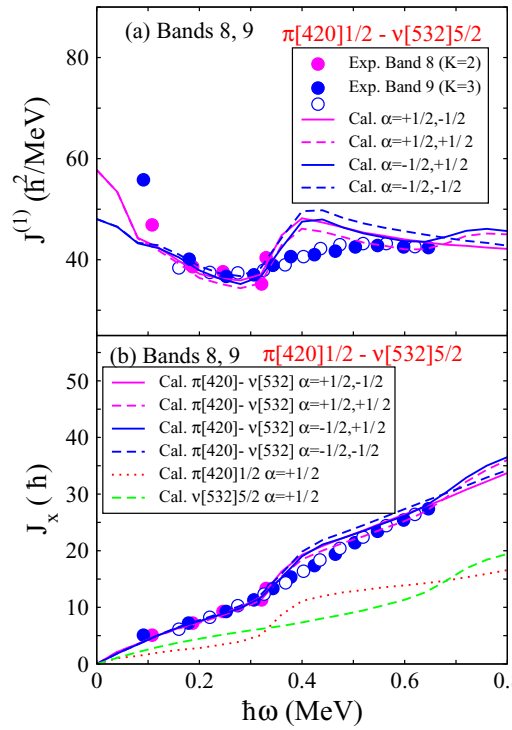

FIG. 18. The same as in Fig. 13 for Bands 8 and 9, for the configuration $\pi[420]1/2^+ \otimes \nu[532]5/2^-$.

can reproduce the moments of inertia of the positive-parity neutron orbitals except the $\nu[413]5/2$ one, which is underestimated, as in the case of ^{119}Ba [20].

Bands 6 and 7 have a behavior which is quite different from that of Bands 3 and 4, presenting weaker crossover transitions, starting and ending at lower frequencies, and being in delayed coincidence with the 66-keV transition which can be placed above the ground state to which we assigned spin-parity $I^{\pi} = 2^{-}$. It is therefore natural to assume lower bandhead spins than those of Bands 3 and 4. In addition, Band 6 has a moment of inertia which decreases with increasing rotational frequency, like Band 1, suggesting the occupation of the $\pi[541]3/2^{-}$ orbital. In fact, only configurations involving the $\pi[541]3/2^{-}$ orbital have calculated moments of inertia in qualitative agreement with Band 6, and the best agreement is obtained by involving the $\alpha = -1/2$ signature partner. We therefore assign the $\pi[541]3/2^{-}(\alpha = -1/2) \otimes \nu[411]3/2^{+}$ configuration to Band 6, which is the GM-favored configuration. The delayed coincidence of Band 6 and 7 with the 66-keV transition suggests similar bandhead spins. Qualitative good agreement for Band 7 is obtained for the $\pi[422]3/2^{+}(\alpha = +1/2) \otimes \nu[532]5/2^{-}$ configuration.

Bands 8–10 are interconnected by several transitions, which fix the relative energies, the spins, the same parity, and also indicate significant mixing. The bands exhibit alignments which saturates at values around $i_x \approx 10\hbar$, indicating the alignment of only one pair of $h_{11/2}$ nucleons. As the behavior of the moments of inertia is very different for configurations involving $h_{11/2}$ protons like those of Bands 1 and 6, and are similar to those involving $h_{11/2}$ neutrons like in Band 3 and 7, we are induced to choose configurations involving the negative-parity $\nu[532]5/2^{-}$ neutron orbital. As one can see in Figs. 17, Band 10 is very well reproduced by the $\pi[422]3/2^{+} \otimes \nu[532]5/2^{-}$ configuration, which is similar to that assigned to Band 7, but involves the $\pi[422]3/2^{+}(\alpha = +1/2)$ orbital with opposite signature. Bands 7 and 10 can therefore be GM partners with $K = 4$ and $K = 1$, respectively. The assigned configurations to Bands 7 and 10 involve $\pi[422]3/2^{+}$ and $\nu[532]5/2^{-}$ orbitals, which have nondegenerate signature partners, while the experimental signature splitting in the two bands is very small. This can be due to axial asymmetry and/or significant interaction between the bands, which are not taken into account in the present calculations. In addition, it is supposed that other potentials, like, e.g., Woods-Saxon, can reproduce better the properties of the bands.

Bands 8 and 9 can involve the $\pi[420]1/2^{+}$ orbital, for which the agreement is not as good as for the other bands, but qualitatively acceptable, see Fig. 18. The coupling with the $\nu[532]5/2^{-}$ orbital leads to the $\pi[420]1/2^{+} \otimes \nu[532]5/2^{-}$ configuration, with GM partners with $K = 2$ and $K = 3$, which are in agreement with the bandheads of Bands 8 and 9, respectively. The presence of the low-$\Omega\pi[420]1/2^{+}$ orbital leads to significant Coriolis mixing between the two bands and can explain the strong interconnecting transitions. However, as one can see in Fig. 18, the present calculations cannot reproduce the smooth up-bending in Band 9. This may be due to a stronger interaction between the two-quasiparticle band and the four-quasiparticle band than in other bands in the backbending region and should be further investigated in the future.

IV. SUMMARY

Summarizing, the present work reports the most complete level schemes from low to high spin in the odd-odd proton-rich lanthanide nuclei. Ten new bands have been identified in the odd-odd ^{118}Cs nucleus. Four new isomers have also been identified, with very different half-lives, one in the nanosecond range, two in the microsecond range, and one with much longer half-life. The analysis of the alignment properties combined with the results of extensive PNC-CSM calculations, led to a global good understanding of the bands structures. The present results constitute a unique set of spectroscopic information which can be used to test state-of-the-art theoretical models aiming to describe strongly deformed proton-rich lanthanide nuclei.

ACKNOWLEDGMENTS

This work has been supported by the China Scholarship Council (CSC), CSC No. 201804910386. This work has been supported by the Academy of Finland under the Finnish Centre of Excellence Programme (2012-2017), by the EU Seventh Framework Programme Project No. 262010 (ENSAR), by the United Kingdom Science and Technology Facilities Council, by the National Research, Development and Innovation Fund of Hungary (Project No. K128947), as well as by the European Regional Development Fund (Contract No. GINOP-2.3.3-15-2016-00034); by the Polish National Science Centre (NCN) Grant No. 2013/10/M/ST2/00427; by the Swedish Research Council under Grant No. 2019-04880; by the Natural Sciences and Engineering Research Council of Canada (NSERC); and by the National Natural Science Foundation of China (Grants No. 11505242, No. 11305220, No. U1732139, No. 11775274, and No. 11575255). The use of germanium detectors from the GAMMAPOOL is acknowledged. I.K. was supported by National Research, Development and Innovation Office-NKFIH, contract number PD 124717.

APPENDIX

Table I with experimental information on the γ-ray transitions of ^{118}Cs obtained in the present experiment.

TABLE I. Experimental information including the γ-ray energies E_γ, energies of the initial levels E_i, relative intensities I_γ, anisotropies $R_{\rm DCO}$ and/or R_{ac}, parameter a_2, parameter a_4, polarization asymmetries A_p extracted following the prescription of Ref. [32], mixing ratios δ, multipolarities, and the spin-parity assignments to the observed states in ^{118}Cs. The transitions listed with increasing energy are grouped in bands. The deduced values for $R_{\rm DCO}$ with a stretched quadrupole gate are ≈1 for stretched quadrupole and ≈0.46 for dipole transitions, while the ratio is close to 1 for a dipole and 2.1 for a quadrupole transition when the gate is set on a dipole transition. The R_{ac} values for stretched dipole and quadrupole transitions are ≈0.8 and ≈1.4.

E_γ (keV)[a]	E_i (keV)	I_γ[b]	$R_{\rm DCO}$[c]	R_{ac}[d]	a_2	a_4	A_p	δ	Mult.	$J_i^\pi \rightarrow J_f^\pi$
Band 1										
132.3	$x+833.3$	35(8)	0.5(2)[e]						$M1+E2$	$(12^+)\rightarrow(11^+)$
200.1	$x+395.1$	1000	0.87(9)[e]				0.14(3)		$E2$	$(10^+)\rightarrow(8^+)$
298.3	$x+1465.4$	6(4)							$(M1+E2)$	$(14^+)\rightarrow(13^+)$
305.2	$x+700.3$	210(25)	0.43(7)[e]		−0.70(10)	0.22(18)	−0.08(4)		$M1+E2$	$(11^+)\rightarrow(10^+)$
308.2	$x+3449.9$	13(4)							$(M1+E2)$	$(19^+)\rightarrow(18^+)$
320.3	$x+2565.6$	28(5)		0.9(3)					$M1+E2$	$(17^+)\rightarrow(16^+)$
333.3	$x+1797.7$	150(35)		0.67(8)			−0.05(1)		$M1+E2$	$(15^+)\rightarrow(14^+)$
334.2	$x+1167.4$	240(65)		0.67(8)					$M1+E2$	$(13^+)\rightarrow(12^+)$
438.2	$x+833.3$	780(25)	1.11(6)[e]				0.10(1)		$E2$	$(12^+)\rightarrow(10^+)$
467.0	$x+1167.4$	100(15)	1.1(3)[e]						$E2$	$(13^+)\rightarrow(11^+)$
629.5	$x+1797.7$	170(45)	1.0(2)[e]						$E2$	$(15^+)\rightarrow(13^+)$
632.1	$x+1465.4$	380(45)	1.0(2)[e]				0.08(3)		$E2$	$(14^+)\rightarrow(12^+)$
767.9	$x+2565.6$	130(20)	1.0(3)[e]						$E2$	$(17^+)\rightarrow(15^+)$
780.0	$x+2245.4$	190(40)	1.0(3)[e]	1.4(2)					$E2$	$(16^+)\rightarrow(14^+)$
884.5	$x+3449.9$	80(16)		1.3(2)					$E2$	$(19^+)\rightarrow(17^+)$
896.0	$x+3141.4$	80(16)	1.1(4)[e]						$E2$	$(18^+)\rightarrow(16^+)$
987.8	$x+4437.7$	90(20)		1.3(2)					$E2$	$(21^+)\rightarrow(19^+)$
1001.0	$x+4142.5$	50(10)		1.5(3)					$E2$	$(20^+)\rightarrow(18^+)$
1076.4	$x+5514.1$	36(10)		1.3(4)					$E2$	$(23^+)\rightarrow(21^+)$
1098.4	$x+5240.9$	22(6)		1.5(7)					$E2$	$(22^+)\rightarrow(20^+)$
1131.0	$x+6645.1$	21(9)		1.5(5)					$E2$	$(25^+)\rightarrow(23^+)$
1177.1	$x+6418.0$	6(3)							$(E2)$	$(24^+)\rightarrow(22^+)$
1195.3	$x+7840.4$	3(2)							$(E2)$	$(27^+)\rightarrow(25^+)$
1220.7	$x+8015.8$	3(2)							$(E2)$	$(27^+)\rightarrow(25^+)$
1257.2	$x+7675.2$	2(1)							$(E2)$	$(26^+)\rightarrow(24^+)$
1281.0	$x+6795.1$	5(4)							$(E2)$	$(25^+)\rightarrow(23^+)$
1283.0	$x+9123.4$	2(1)							$(E2)$	$(29^+)\rightarrow(27^+)$
1296.0	$x+9311.8$	1(1)							$(E2)$	$(29^+)\rightarrow(27^+)$
1338.9	$x+9014.1$	1(1)							$(E2)$	$(28^+)\rightarrow(26^+)$
Transitions depopulating the isomeric states (8^+) and (7^+)										
69.3	$x+195$	33(9)							$(M1+E2)$	$(8^+)\rightarrow(7^+)$
46.3	$x+125.7$									$(7^+)\rightarrow(5,6)$
61.4	$x+61.4$									$(7^+)\rightarrow(5,6)$
64.7	$x+125.7$									$(5,6)\rightarrow(7^-)$
79.0	$x+79.0$									$(5,6)\rightarrow(7^-)$
126.0	$x+125.7$								$(E1)$	$(7^+)\rightarrow(7^-)$
Band γ										
620.2	$x+1873.8$	10(5)								
Band $\gamma\rightarrow$ Band 1										
553.3	$x+1253.6$	18(8)								$\rightarrow(11^+)$
708.0	$x+1875.4$	11(6)								$\rightarrow(13^+)$
735.4	$x+1568.7$	17(8)								$\rightarrow(12^+)$
796.2	$x+1963.6$	11(6)								$\rightarrow(13^+)$
872.8	$x+1706.1$	17(9)								$\rightarrow(12^+)$
902.5	$x+2069.9$	5(2)								$\rightarrow(13^+)$

TABLE I. *(Continued.)*

E_γ (keV)[a]	E_i (keV)	I_γ[b]	$R_{\rm DCO}$[c]	R_{ac}[d]	a_2	a_4	A_p	δ	Mult.	$J_i^\pi \to J_f^\pi$
980.3	$x + 1680.6$	6(2)								$\to (11^+)$
1016.2	$x + 1849.5$	10(5)								$\to (12^+)$
1108.0	$x + 1808.0$	6(3)								$\to (11^+)$
Band 2										
550.8	$x + 1614.5$	3(2)							$(E2)$	$(13^+) \to (11^+)$
693.3	$x + 2737.3$	10(3)							$(E2)$	$(16^+) \to (14^+)$
695.0	$x + 2309.5$	4(2)							$(E2)$	$(15^+) \to (13^+)$
824.0	$x + 3133.5$	8(6)							$(E2)$	$(17^+) \to (15^+)$
824.8	$x + 3562.3$	19(7)							$(E2)$	$(18^+) \to (16^+)$
913.5	$x + 4047.0$	5(4)							$(E2)$	$(19^+) \to (17^+)$
937.8	$x + 4500.1$	10(5)							$(E2)$	$(20^+) \to (18^+)$
Band 2 $\to$ Band 1										
229.5	$x + 1062.8$	6(2)							$(M1+E2)$	$(11^+) \to (12^+)$
667.6	$x + 1062.8$	7(3)							$(M1+E2)$	$(11^+) \to (10^+)$
781.5	$x + 1614.5$	12(4)							$(M1+E2)$	$(13^+) \to (12^+)$
844.1	$x + 2309.5$	12(9)							$(M1+E2)$	$(15^+) \to (14^+)$
877.3	$x + 2044.7$	34(9)							$(M1+E2)$	$(14^+) \to (13^+)$
939.3	$x + 2737.3$	22(15)							$(M1+E2)$	$(16^+) \to (15^+)$
997.0	$x + 3562.3$	13(4)							$(M1+E2)$	$(18^+) \to (17^+)$
Band 3										
182.9	$x + 182.9$	450(70)	1.2(2)[f]	0.91(5)	−0.15(9)	0.31(17)	−0.03(2)	0.10(35)	$M1+E2$	$(8^-) \to (7^-)$
265.5	$x + 448.4$	280(50)	1.0(2)[f]	0.9(1)	−0.18(2)	0.10(2)	−0.2(1)	0.00(20)	$M1+E2$	$(9^-) \to (8^-)$
288.3	$x + 736.7$	150(26)	1.0(2)[f]	0.74(8)	−0.00(30)	0.11(57)	−0.3(2)	0.10(20)	$M1+E2$	$(10^-) \to (9^-)$
310.5	$x + 1047.3$	90(18)	0.9(1)[f]	1.0(2)					$M1+E2$	$(11^-) \to (10^-)$
330.8	$x + 1378.5$	68(14)	1.1(2)[f]	1.0(2)					$M1+E2$	$(12^-) \to (11^-)$
347.9	$x + 1726.4$	45(9)		0.7(2)					$M1+E2$	$(13^-) \to (12^-)$
362.6	$x + 2089.1$	27(6)		0.9(3)					$M1+E2$	$(14^-) \to (13^-)$
370.0	$x + 2459.2$	11(3)		1.0(4)					$M1+E2$	$(15^-) \to (14^-)$
392.4	$x + 3245.6$	10(3)							$(M1+E2)$	$(17^-) \to (16^-)$
394.2	$x + 2853.7$	7(2)							$(M1+E2)$	$(16^-) \to (15^-)$
405.1	$x + 3651.4$	3(2)							$(M1+E2)$	$(18^-) \to (17^-)$
448.6	$x + 448.4$	16(5)							$(E2)$	$(9^-) \to (7^-)$
554.5	$x + 736.7$	27(7)		1.3(5)					$E2$	$(10^-) \to (8^-)$
599.2	$x + 1047.3$	46(9)		1.5(4)					$E2$	$(11^-) \to (9^-)$
642.4	$x + 1378.5$	45(9)		1.2(3)					$E2$	$(12^-) \to (10^-)$
679.1	$x + 1726.4$	50(10)	1.6(5)[f]	1.2(3)					$E2$	$(13^-) \to (11^-)$
710.6	$x + 2089.1$	36(7)		1.3(3)					$E2$	$(14^-) \to (12^-)$
732.8	$x + 2459.2$	25(5)		1.4(3)					$E2$	$(15^-) \to (13^-)$
764.6	$x + 2853.7$	19(9)		1.6(8)					$E2$	$(16^-) \to (14^-)$
785.3	$x + 3245.6$	5(4)							$(E2)$	$(17^-) \to (15^-)$
797.7	$x + 3651.4$	7(2)							$(E2)$	$(18^-) \to (16^-)$
844.3	$x + 4088.8$	8(3)							$(E2)$	$(19^-) \to (17^-)$
869.9	$x + 4521.3$	7(3)							$(E2)$	$(20^-) \to (18^-)$
899.6	$x + 4988.4$	3(2)							$(E2)$	$(21^-) \to (19^-)$
959.4	$x + 5480.7$	2(1)							$(E2)$	$(22^-) \to (20^-)$
1011.9	$x + 6000.3$	1(1)							$(E2)$	$(23^-) \to (21^-)$
Band 4										
192.6	$y + 192.6$	550(150)	0.93(7)[f]	0.86(4)	−0.22(7)	0.14(12)		0.00(20)	$M1+E2$	$(7^+) \to (6^+)$
236.4	$y + 429.1$	525(100)	1.11(7)[f]	0.82(3)	−0.22(5)	0.08(10)	−0.02(1)	0.00(15)	$M1+E2$	$(8^+) \to (7^+)$
274.6	$y + 703.8$	300(50)	1.11(9)[f]	0.85(4)	−0.11(18)	0.06(34)	−0.07(2)	0.10(10)	$M1+E2$	$(9^+) \to (8^+)$
307.0	$y + 1011.1$	250(50)	0.97(9)[f]	0.89(5)	−0.12(6)	0.23(11)	−0.02(1)	0.10(25)	$M1+E2$	$(10^+) \to (9^+)$
335.3	$y + 1346.1$	180(35)	1.0(2)[f]	0.87(5)	−0.38(6)	−0.00(10)		-0.10(15)	$M1+E2$	$(11^+) \to (10^+)$
358.5	$y + 1704.5$	70(14)	1.1(1)[f]	0.9(3)					$M1+E2$	$(12^+) \to (11^+)$
374.9	$y + 2079.8$	32(9)		0.8(2)					$M1+E2$	$(13^+) \to (12^+)$
387.9	$y + 2467.6$	22(6)		1.0(3)					$M1+E2$	$(14^+) \to (13^+)$

TABLE I. *(Continued.)*

E_γ (keV)[a]	E_i (keV)	I_γ[b]	$R_{\rm DCO}$[c]	R_{ac}[d]	a_2	a_4	A_p	δ	Mult.	$J_i^\pi \rightarrow J_f^\pi$
395.1	$y+2863.2$	21(5)		0.9(4)					$M1+E2$	$(15^+) \rightarrow (14^+)$
401.8	$y+3263.9$	8(2)		0.9(5)					$M1+E2$	$(16^+) \rightarrow (15^+)$
405.3	$y+3669.9$	6(2)							$(M1+E2)$	$(17^+) \rightarrow (16^+)$
418.4	$y+4087.1$	4(2)							$(M1+E2)$	$(18^+) \rightarrow (17^+)$
430.0	$y+4518.8$	5(3)							$(M1+E2)$	$(19^+) \rightarrow (18^+)$
430.0	$y+429.1$	60(20)	1.7(8)[f]						$E2$	$(8^+) \rightarrow (6^+)$
511.7	$y+703.8$	60(10)	2.0(5)[f]				0.12(6)		$E2$	$(9^+) \rightarrow (7^+)$
582.7	$y+1011.1$	110(20)	1.6(5)[f]	1.35(8)					$E2$	$(10^+) \rightarrow (8^+)$
641.8	$y+1346.1$	100(20)	2.0(4)[f]				0.05(3)		$E2$	$(11^+) \rightarrow (9^+)$
693.3	$y+1704.5$	110(30)	1.2(4)[e]				0.07(2)		$E2$	$(12^+) \rightarrow (10^+)$
733.8	$y+2079.8$	83(17)	0.8(2)[e]	1.4(1)					$E2$	$(13^+) \rightarrow (11^+)$
763.1	$y+2467.6$	90(20)	1.1(5)[e]	1.4(2)					$E2$	$(14^+) \rightarrow (12^+)$
783.6	$y+2863.2$	56(11)		1.4(2)					$E2$	$(15^+) \rightarrow (13^+)$
796.3	$y+3263.9$	53(12)	1.3(5)[e]	1.4(2)					$E2$	$(16^+) \rightarrow (14^+)$
806.7	$y+3669.9$	42(10)		1.3(2)					$E2$	$(17^+) \rightarrow (15^+)$
823.2	$y+4087.1$	30(8)		1.5(3)					$E2$	$(18^+) \rightarrow (16^+)$
848.9	$y+4518.8$	28(7)		1.2(3)					$E2$	$(19^+) \rightarrow (17^+)$
Band 5										
113.5	$y+1671.5$	5(3)							$(M1+E2)$	$(11^+) \rightarrow (10^+)$
336.0	$y+2355.8$	5(3)							$(M1+E2)$	$(13^+) \rightarrow (12^+)$
348.8	$y+2020.1$	9(4)							$(M1+E2)$	$(12^+) \rightarrow (11^+)$
640.9	$y+2661.0$	9(5)							$(E2)$	$(14^+) \rightarrow (12^+)$
684.3	$y+2355.8$	26(10)		1.4(5)					$E2$	$(13^+) \rightarrow (11^+)$
743.2	$y+3099.0$	10(6)							$(E2)$	$(15^+) \rightarrow (13^+)$
814.0	$y+3913.0$	5(4)							$(E2)$	$(17^+) \rightarrow (15^+)$
Band 5$\rightarrow$ Band 4										
651.6	$y+2355.8$	12(5)							$(M1+E2)$	$(13^+) \rightarrow (12^+)$
660.4	$y+1671.5$	34(13)		0.9(3)					$M1+E2$	$(11^+) \rightarrow (10^+)$
674.0	$y+2020.1$	16(7)							$(M1+E2)$	$(12^+) \rightarrow (11^+)$
852.3	$y+1556.1$	10(6)							$(M1+E2)$	$(10^+) \rightarrow (9^+)$
931.2	$y+1360.3$	17(5)							$(M1+E2)$	$(9^+) \rightarrow (8^+)$
Band 6										
62.6	128.8	20(10)		0.9(5)					$M1+E2$	$(4^-) \rightarrow (3^-)$
89.1	217.9	60(20)		0.63(9)	$-0.93(4)$	0.32(6)		$-1.6(3)$ or $-0.4(3)$	$M1+E2$	$(5^-) \rightarrow (4^-)$
115.9	333.8	80(20)	0.9(4)[f]	0.91(5)	$-0.52(19)$	0.31(7)		$-3.6(13)$ or $-0.1(5)$	$M1+E2$	$(6^-) \rightarrow (5^-)$
141.8	475.7	80(20)		0.63(9)	$-0.49(10)$	0.29(17)		$-4.0(16)$ or$-0.1(4)$	$M1+E2$	$(7^-) \rightarrow (6^-)$
171.4	647.1	50(20)	0.8(4)[f]	0.91(5)					$M1+E2$	$(8^-) \rightarrow (7^-)$
199.5	846.6	45(15)		0.73(9)					$M1+E2$	$(9^-) \rightarrow (8^-)$
227.8	1074.4	30(10)	0.8(4)[f]	0.7(2)					$M1+E2$	$(10^-) \rightarrow (9^-)$
258.3	475.7	10(5)							$(E2)$	$(7^-) \rightarrow (5^-)$
261.7	1336.4	8(3)							$(M1+E2)$	$(11^-) \rightarrow (10^-)$
303.2	1639.6	7(3)							$(M1+E2)$	$(12^-) \rightarrow (11^-)$
311.6	1951.3	5(3)							$(M1+E2)$	$(13^-) \rightarrow (12^-)$
312.8	647.1	4(3)							$(E2)$	$(8^-) \rightarrow (6^-)$
339.0	2290.3	4(3)							$(M1+E2)$	$(14^-) \rightarrow (13^-)$
370.8	846.6	6(4)							$(E2)$	$(9^-) \rightarrow (7^-)$
374.0	2664.3	3(2)							$(M1+E2)$	$(15^-) \rightarrow (14^-)$
427.8	1074.4	3(2)							$(E2)$	$(10^-) \rightarrow (8^-)$
490.7	1336.4	3(2)							$(E2)$	$(11^-) \rightarrow (9^-)$
615.3	1951.3	2(1)							$(E2)$	$(13^-) \rightarrow (11^-)$
Transition depopulating the isomeric band-head 3^- of Band 6										
65.9	65.9								$(M1)$	$(3^-) \rightarrow (2^-)$

TABLE I. *(Continued.)*

E_γ (keV)[a]	E_i (keV)	I_γ[b]	$R_{\rm DCO}$[c]	R_{ac}[d]	a_2	a_4	A_p	δ	Mult.	$J_i^\pi \rightarrow J_f^\pi$
Levels populating the 9^-, 10^- and 11^- states of Band 6										
248.3	1094.9	5(4)								$\rightarrow (9^-)$
254.5	1348.7	3(2)								
274.0	1348.7	14(6)								$\rightarrow (10^-)$
502.5	1348.7	9(5)								$\rightarrow (9^-)$
Band 7										
118.8	263.7	60(23)		0.7(1)					$M1+E2$	$(5^-) \rightarrow (4^-)$
152.0	415.7	50(20)	1.3(5)[f]	0.80(9)					$M1+E2$	$(6^-) \rightarrow (5^-)$
180.4	596.1	45(14)		0.74(8)					$M1+E2$	$(7^-) \rightarrow (6^-)$
213.5	809.6	30(10)		0.9(1)					$M1+E2$	$(8^-) \rightarrow (7^-)$
238.3	1047.9	25(9)		0.9(2)					$M1+E2$	$(9^-) \rightarrow (8^-)$
263.9	1311.8	17(7)		0.8(3)					$M1+E2$	$(10^-) \rightarrow (9^-)$
282.7	1594.5	9(3)							$(M1+E2)$	$(11^-) \rightarrow (10^-)$
310.2	1904.7	4(2)							$(M1+E2)$	$(12^-) \rightarrow (11^-)$
320.8	2225.9	2(1)							$(M1+E2)$	$(13^-) \rightarrow (12^-)$
333.0	596.1	10(6)							$(E2)$	$(7^-) \rightarrow (5^-)$
334.1	2560.3	1(1)							$(M1+E2)$	$(14^-) \rightarrow (13^-)$
342.5	2902.4	1(1)							$(M1+E2)$	$(15^-) \rightarrow (14^-)$
394.9	809.6	3(2)							$(E2)$	$(8^-) \rightarrow (6^-)$
452.3	1047.9	5(3)							$(E2)$	$(9^-) \rightarrow (7^-)$
502.8	1311.8	6(3)							$(E2)$	$(10^-) \rightarrow (8^-)$
547.3	1594.5	2(1)							$(E2)$	$(11^-) \rightarrow (9^-)$
592.8	1904.7	2(1)							$(E2)$	$(12^-) \rightarrow (10^-)$
631.8	2225.9	2(1)							$(E2)$	$(13^-) \rightarrow (11^-)$
655.9	2560.3	1(1)							$(E2)$	$(14^-) \rightarrow (12^-)$
676.0	2902.4	1(1)							$(E2)$	$(15^-) \rightarrow (13^-)$
Band 7 $\rightarrow$ Band 6										
79.0	144.9	30(20)		0.79(8)					$M1+E2$	$(4^-) \rightarrow (3^-)$
Band 8										
233.3	312.6	30(10)							$(E2)$	$(6^-) \rightarrow (4^-)$
388.9	701.3	6(3)							$(E2)$	$(8^-) \rightarrow (6^-)$
504.5	1205.8	5(3)							$(E2)$	$(10^-) \rightarrow (8^-)$
653.9	1859.7	4(3)							$(E2)$	$(12^-) \rightarrow (10^-)$
669.0	2528.7	2(2)							$(E2)$	$(14^-) \rightarrow (12^-)$
Band 8 $\rightarrow$ Band 9										
36.7	79.4	30(20)							$(M1+E2)$	$(4^-) \rightarrow (3^-)$
145.0	312.6	90(30)		0.8(2)					$M1+E2$	$(6^-) \rightarrow (5^-)$
195.8	701.3	5(4)							$(M1+E2)$	$(8^-) \rightarrow (7^-)$
Band 9										
74.8	117.3	80(40)		0.5(2)					$M1+E2$	$(4^-) \rightarrow (3^-)$
125.0	167.6	10(5)							$(E2)$	$(5^-) \rightarrow (3^-)$
145.7	313.8	40(10)		0.7(2)					$M1+E2$	$(6^-) \rightarrow (5^-)$
182.3	687.6	24(8)							$(M1+E2)$	$(8^-) \rightarrow (7^-)$
191.7	505.4	20(10)							$(M1+E2)$	$(7^-) \rightarrow (6^-)$
197.0	313.8	75(20)		1.4(5)					$E2$	$(6^-) \rightarrow (4^-)$
245.4	1205.5	11(20)							$(M1+E2)$	$(10^-) \rightarrow (9^-)$
272.1	959.2	32(15)							$(M1+E2)$	$(9^-) \rightarrow (8^-)$
315.2	1520.3	19(9)							$(M1+E2)$	$(11^-) \rightarrow (10^-)$
338.1	505.4	32(12)		1.3(4)					$E2$	$(7^-) \rightarrow (5^-)$
373.8	687.6	160(70)	0.9(3)[e]	1.2(2)					$E2$	$(8^-) \rightarrow (6^-)$
453.6	959.2	100(40)	1.9(4)[f]	1.3(3)					$E2$	$(9^-) \rightarrow (7^-)$
518.0	1205.5	110(40)		1.3(2)					$E2$	$(10^-) \rightarrow (8^-)$
561.0	1520.3	80(30)		1.6(3)					$E2$	$(11^-) \rightarrow (9^-)$
621.7	1827.2	70(20)		1.2(3)					$E2$	$(12^-) \rightarrow (10^-)$
660.5	2180.8	70(20)		1.4(3)					$E2$	$(13^-) \rightarrow (11^-)$

TABLE I. *(Continued.)*

E_γ (keV)[a]	E_i (keV)	I_γ[b]	$R_{\rm DCO}$[c]	R_{ac}[d]	a_2	a_4	A_p	δ	Mult.	$J_i^\pi \rightarrow J_f^\pi$
693.6	2520.8	50(20)		1.3(3)					$E2$	$(14^-) \rightarrow (12^-)$
743.4	2924.2	34(11)		1.6(5)					$E2$	$(15^-) \rightarrow (13^-)$
763.9	3284.7	35(14)		1.6(6)					$E2$	$(16^-) \rightarrow (14^-)$
813.2	3737.4	13(4)		1.4(5)					$E2$	$(17^-) \rightarrow (15^-)$
853.1	4137.8	11(3)							$(E2)$	$(18^-) \rightarrow (16^-)$
876.4	4613.8	11(3)							$(E2)$	$(19^-) \rightarrow (17^-)$
935.9	5073.7	14(4)							$(E2)$	$(20^-) \rightarrow (18^-)$
953.8	5567.6	9(3)							$(E2)$	$(21^-) \rightarrow (19^-)$
1013.1	6086.8	13(4)							$(E2)$	$(22^-) \rightarrow (20^-)$
1041.1	6608.7	8(3)							$(E2)$	$(23^-) \rightarrow (21^-)$
1097.9	7184.7	3(1)							$(E2)$	$(24^-) \rightarrow (22^-)$
1133.3	7742.0	6(3)							$(E2)$	$(25^-) \rightarrow (23^-)$
1197.8	8382.5	2(1)							$(E2)$	$(26^-) \rightarrow (24^-)$
1241.2	8983.2	2(1)							$(E2)$	$(27^-) \rightarrow (25^-)$
1294.4	9676.9	1(1)							$(E2)$	$(28^-) \rightarrow (26^-)$
Band 9 → Band 8										
37.3	117.3	17(10)							$(M1+E2)$	$(4^-) \rightarrow (4^-)$
42.7	42.7	40(20)							$(M1+E2)$	$(3^-) \rightarrow (2^-)$
88.2	167.6	66(30)	1.0(2)[f]	0.6(2)					$M1+E2$	$(5^-) \rightarrow (4^-)$
192.8	505.4	20(10)							$(M1+E2)$	$(7^-) \rightarrow (6^-)$
Band 9 → Band 10										
64.9	313.8	30(20)		0.5(2)					$M1+E2$	$(6^-) \rightarrow (5^-)$
135.8	687.6	9(4)							$(M1+E2)$	$(8^-) \rightarrow (7^-)$
407.5	959.2	18(9)							$(E2)$	$(9^-) \rightarrow (7^-)$
Band 10										
198.1	750.7	5(4)							$(M1+E2)$	$(8^-) \rightarrow (7^-)$
298.1	1048.2	4(3)							$(M1+E2)$	$(9^-) \rightarrow (8^-)$
303.3	551.6	16(8)							$(E2)$	$(7^-) \rightarrow (5^-)$
496.6	1048.2	19(10)		1.3(3)					$E2$	$(9^-) \rightarrow (7^-)$
585.4	1336.1	30(15)		1.3(2)					$E2$	$(10^-) \rightarrow (8^-)$
631.4	1679.6	18(10)							$(E2)$	$(11^-) \rightarrow (9^-)$
688.5	2024.6	20(10)		1.3(4)					$E2$	$(12^-) \rightarrow (10^-)$
711.1	2390.7	16(9)							$(E2)$	$(13^-) \rightarrow (11^-)$
726.8	2751.4	4(3)							$(E2)$	$(14^-) \rightarrow (12^-)$
739.5	3130.2	11(7)							$(E2)$	$(15^-) \rightarrow (13^-)$
779.4	3909.6	7(4)							$(E2)$	$(17^-) \rightarrow (15^-)$
828.0	4737.6	4(2)							$(E2)$	$(19^-) \rightarrow (17^-)$
Band 10 → Band 8										
436.9	750.7	40(20)		1.3(2)					$E2$	$(8^-) \rightarrow (6^-)$
Band 10 → Band 9										
131.5	248.8	100(50)		0.8(2)					$M1+E2$	$(5^-) \rightarrow (4^-)$
237.8	551.6	70(30)	1.0(3)[f]	0.7(1)					$M1+E2$	$(7^-) \rightarrow (6^-)$
360.3	1048.2	6(4)							$(M1+E2)$	$(9^-) \rightarrow (8^-)$
384.0	551.6	7(4)							$(E2)$	$(7^-) \rightarrow (5^-)$

[a]The error on the transition energies is 0.3 keV for transitions below 500 keV, 0.7 keV for transitions between 500 and 1000 keV, and 1.0 keV for transitions above 1000 keV. The error on the transition transition energies is 1.0 keV for the transition intensities less than 10.

[b]Relative intensities corrected for efficiency, normalized to the intensity of the 200.1 keV ($10^+ \rightarrow 8^+$ of Band 1) transition [14]. The transition intensities were obtained from a combination of total projection and gated spectra.

[c]$R_{\rm DCO}$ has been deduced from an asymmetric γ-γ coincidence matrix sorted with the detectors at 157.6° on one axis, and detectors at ≈90° on the other axis. The tentative spin-parity of the states are given in parentheses.

[d]R_{ac} has been deduced from two asymmetric γ-γ coincidence matrices sorted with the detectors at 133.6° and 157.6° on one axis, and detectors at ≈90° on the other axis. The tentative spin-parity of the states are given in parentheses.

[e]DCO ratio from spectrum gated on stretched quadrupole transition.

[f]DCO ratio from spectrum gated on stretched dipole transition.

[1] B. Xiong and Y. Wang, At. Data Nucl. Data Tables **125**, 193 (2019).
[2] ENSDF, NNDC Online Data Service, ENSDF database, http://www.nndc.bnl.gov/ensdf/.
[3] B. Cederwall *et al.*, Nucl. Phys. A **542**, 454 (1992).
[4] C. B. Moon, S. J. Chae, J. H. Ha, T. Komatsubara, Y. Sasaki, T. Jumatsu, K. Yamada, K. Satou, and K. Furuno, Nucl. Phys. A **696**, 45 (2001).
[5] P. T. Wady *et al.*, Phys. Rev. C **85**, 034329 (2012).
[6] J. F. Smith *et al.*, Phys. Rev. C **73**, 061303(R) (2006).
[7] J. F. Smith *et al.*, Phys. Rev. C **74**, 034310 (2006).
[8] J. F. Smith *et al.*, Phys. Lett. B **406**, 17 (1997).
[9] R. D. Page, P. J. Woods, R. A. Cunningham, T. Davinson, N. J. Davis, A. N. James, K. Livingston, P. J. Sellin, and A. C. Shotter, Phys. Rev. Lett. **72**, 1798 (1994).
[10] L. Cartegni *et al.*, Phys. Rev. C **85**, 014312 (2012).
[11] F. Ames *et al.*, Nucl. Phys. A **651**, 3 (1999).
[12] J. Genevey-Rivier, A. Charvet, G. Marguier, C. Richard-Serre, J. D'Auria, A. Huck, G. Klotz, A. Knipper, and G. Walter (ISOLDE Collaboration), Nucl. Phys. A **283**, 45 (1977).
[13] C. Thibault *et al.*, Nucl. Phys. A **367**, 1 (1981).
[14] F. Lidén *et al.*, Nucl. Phys. A **550**, 365 (1992).
[15] F. R. Xu, P. M. Walker, J. A. Sheikh, and R. Wyss, Phys. Lett. B **435**, 257 (1998).
[16] H. L. Liu, F. R. Xu, S. W. Xu, R. Wyss, and P. M. Walker, Phys. Rev. C **76**, 034313 (2007).
[17] C. J. J. Gallacher and S. A. Moszkowski, Phys. Rev. **111**, 1282 (1958).
[18] A. K. Jain, B. Maheshwari, S. Garg, M. Patial, and B. Singh, Nucl. Data Sheets **128**, 1 (2015).
[19] K. K. Zheng *et al.*, Phys. Rev. C **104**, 044305 (2021).
[20] K. K. Zheng *et al.*, Phys. Rev. C **104**, 014326 (2021).
[21] J. Pakarinen *et al.*, Eur. Phys. J. A **56**, 149 (2020).
[22] J. Sarén *et al.*, Nucl. Instrum. Methods Phys. Res., Sect. B **266**, 4196 (2008).
[23] K. K. Zheng *et al.*, Eur. Phys. J. A (to be published).
[24] K. K. Zheng *et al.*, Phys. Lett. B **822**, 136645 (2021).
[25] J. Y. Zeng, T. H. Jin, and Z. J. Zhao, Phys. Rev. C **50**, 1388 (1994).
[26] Z. H. Zhang, M. Huang, and A. V. Afanasjev, Phys. Rev. C **101**, 054303 (2020).
[27] Y. Liu, J. Lu, Y. Ma, G. Zhao, H. Zheng, and S. Zhou, Phys. Rev. C **58**, 1849 (1998).
[28] C. B. Moon, G. D. Dracoulis, R. A. Bark, A. P. Byrne, P. A. Davidson, A. N. Wilson, A. M. Baxter, T. Kibédi, and G. J. Lane, J. Korean Phys. Soc. **43**, S100 (2003).
[29] P. Bednarczyk, Z. Phys. A: Hadrons Nucl. **346**, 325 (1993).
[30] T. Bengtsson and I. Ragnarsson, Nucl. Phys. A **436**, 14 (1985).
[31] C. B. Moon, T. Komatsubara, and K. Furuno, Nucl. Phys. A **730**, 3 (2004).
[32] K. Starosta *et al.*, Nucl. Instrum. Methods Phys. Res., Sect. A **423**, 16 (1999).